



# Atmospheric and surface observations during the Saint John River Experiment on Cold Season Storms (SAJESS)

Hadleigh D. Thompson<sup>1</sup>, Julie M. Thériault<sup>1</sup>, Stephen J. Déry<sup>2</sup>, Ronald E. Stewart<sup>3</sup>,  
Dominique Boisvert<sup>1</sup>, Lisa Rickard<sup>2</sup>, Nicolas R. Leroux<sup>1</sup>, Matteo Colli<sup>4</sup>, and Vincent Vionnet<sup>5</sup>

<sup>1</sup>Department of Earth and Atmospheric Sciences, Centre ESCER, Université du Québec à Montréal,  
Montréal, Quebec, H3C 3P8, Canada

<sup>2</sup>Department of Geography, Earth and Environmental Sciences and Natural Resources and Environmental  
Studies Program, University of Northern British Columbia, Prince George, British Columbia, V2N 4Z9, Canada

<sup>3</sup>Department of Environment and Geography, University of Manitoba, Winnipeg, Manitoba, R3T 2N2, Canada

<sup>4</sup>Artys Srl, Piazza della Vittoria, 9/3, 16121 Genoa, Italy

<sup>5</sup>Meteorological Research Division, Environment and Climate Change Canada, Dorval,  
Quebec, H9P 1J3, Canada

**Correspondence:** Julie M. Thériault (theriault.julie@uqam.ca)

Received: 16 February 2023 – Discussion started: 28 March 2023

Revised: 6 October 2023 – Accepted: 10 October 2023 – Published: 19 December 2023

**Abstract.** The amount and the phase of cold-season precipitation accumulating in the upper Saint John River (SJR) basin are critical factors in determining spring runoff, ice jams, and flooding. To study the impact of winter and spring storms on the snowpack in the upper SJR basin, the Saint John River Experiment on Cold Season Storms (SAJESS) was conducted during winter–spring 2020–2021. Here, we provide an overview of the SAJESS study area, field campaign, and data collected. The upper SJR basin represents 41 % of the entire SJR watershed and encompasses parts of the US state of Maine and the Canadian provinces of Quebec and New Brunswick. In early December 2020, meteorological instruments were co-located with an Environment and Climate Change Canada station near Edmundston, New Brunswick. This included a separate weather station for measuring standard meteorological variables, an optical disdrometer, and a micro rain radar. This instrumentation was augmented during an intensive observation period that also included upper-air soundings, surface weather observations, a multi-angle snowflake camera, and macrophotography of solid hydrometeors throughout March and April 2021. During the study, the region experienced a lower-than-average snowpack that peaked at  $\sim 65$  cm, with a total of 287 mm of precipitation (liquid-equivalent) falling between December 2020 and April 2021, a 21 % lower amount of precipitation than the climatological normal. Observers were present for 13 storms during which they conducted 183 h of precipitation observations and took more than 4000 images of hydrometeors. The inclusion of local volunteers and schools provided an additional 1700 measurements of precipitation amounts across the area. The resulting datasets are publicly available from the Federated Research Data Repository at <https://doi.org/10.20383/103.0591> (Thompson et al., 2023). We also include a synopsis of the data management plan and a brief assessment of the rewards and challenges of conducting the field campaign and utilizing community volunteers for citizen science.

## 1 Introduction

The Saint John River Experiment on Cold Season Storms (SAJESS) focused on cold-region processes related to winter and spring storms over the transboundary upper Saint John River basin, located on the border of Maine (ME) and the provinces of Quebec (QC) and New Brunswick (NB). The Saint John River, known as the Wolastoq by local Indigenous communities, is 673 km long and drops 480 m in elevation from its source at the Little John River (ME) down to the Bay of Fundy (Fig. 1). The Saint John River watershed covers 55 000 km<sup>2</sup>, with 36 % located in the United States, although, here we define the upper Saint John River basin as the area that drains into the Saint John River above Grand Falls, NB. Economically important to the region, the river provides flow for five hydroelectric facilities, with development being overseen by the International Joint Commission (Kenny and Secord, 2010).

A concern of emergency managers along the Saint John River is the risk of catastrophic flooding, particularly from significant snowmelt. Such flooding events occurred in 2008, 2018, and again in 2019 and were in the annual top 10 Canadian weather disasters identified by Environment and Climate Change Canada (ECCC) (ECCC, 2017, 2019, 2020). Although this sub-catchment covers an area of 22 600 km<sup>2</sup>, most of the research focusing on the Saint John River does so by examining the lower reaches and associated lakes, wetlands, and tidal estuaries. There is therefore a paucity of both hydrological knowledge of the upper basin, as noted by Budhathoki et al. (2022), and meteorological stations (only two within the upper SJR basin) (also see Fortin and Dubreuil, 2020).

There have been several previous cold-season precipitation studies in North America. These include a comparison between orographic winter storms in the San Juan Mountains and Sierra Nevada by Marwitz (1986), the Canadian Atlantic Storms Program (Stewart et al., 1987; Stewart, 1991) that investigated the synoptic and mesoscale structure of Canadian east-coast winter storms, and field campaigns such as the meteorological monitoring network established for the Vancouver 2010 winter Olympics (Joe et al., 2014), and the Olympic Mountains experiment (OLYMPEX) that studied the modification of Pacific storms by coastal mountain ranges (Houze et al., 2017). Notably, the Vancouver Olympics network utilized a first-generation hotplate precipitation gauge, and while OLYMPEX used similar instrumentation to SAJESS such as disdrometers, weighing rain gauges, and micro rain radars, they also employed instrumented aircraft and a greater range of radar options. Ongoing research into east-coast snowstorm-producing cyclones is being undertaken by the Investigation of Microphysics and Precipitation for Atlantic Coast-Threatening Snowstorms (IMPACTS) campaign (McMurdie et al., 2022). Similar to OLYMPEX, IMPACTS combines surface observations and measurements with airborne remote sensing instruments. In

terms of field projects, SAJESS compares closest to the recent (2019) Storms and Precipitation Across the continental Divide experiment (SPADE) (Thériault et al., 2021a, 2022), adopting the methods of manual observations, macrophotography, and micro rain radar and disdrometer deployment, although we built on SPADE by adding a distributed network of temperature and precipitation measurements and upper-air observations.

Locally, previous studies encompassing the Saint John River basin have focused on flooding (Newton and Burrell, 2016), including rain-on-snow events (Buttle et al., 2016), and the analysis and modelling of ice jams that may increase in frequency in future climate scenarios (Beltaos et al., 2003). Despite these hazards, no studies of storms and precipitation and their impact on snowpack evolution have been conducted in this region.

The SAJESS dataset contains meteorological and precipitation data that were collected at a Fixed Station from 1 December 2020 until 30 April 2021 and an intensive observation period (IOP) that took place from 8 March to 30 April 2021. The objective of this paper is to describe the data collected during SAJESS, provide examples of the measurements and how they can be combined to broaden the picture of meteorological conditions observed, and illustrate to stakeholders and potential users the importance of the field campaign and dataset.

The paper is organized as follows: the sites used during SAJESS are described in Sect. 2; the instruments, manual observations, and other sources of data are detailed in Sect. 3; an overview of data processing, management, and validity, along with examples of data collected throughout SAJESS, is presented in Sect. 4; and a summary, including a discussion on potential future analyses, is given in Sect. 5.

## 2 Site descriptions

### 2.1 Overview

To observe the spatial and temporal variability in precipitation amount and phase across the study area, a broad range of techniques was employed: first, a semi-permanent “precipitation phase observatory” was installed to record meteorological data from December 2020 to April 2021. This site became known as the “Fixed Station” and was co-located with the permanent ECCC station, north of Edmundston (Fig. 1). Second, the Mobile Urban Weather Station (MUST), a modified enclosed trailer provided by the Université du Québec à Montréal (UQAM), was situated at the confluence of the Madawaska and Saint John rivers for the IOP during April and May 2021. The MUST was located on property provided by the City of Edmundston and was used as a base for graduate students and volunteers to record manual observations, capture macrophotography images of hydrometeors, and release sounding balloons for upper-air observations. Finally, community volunteers were engaged by providing lo-

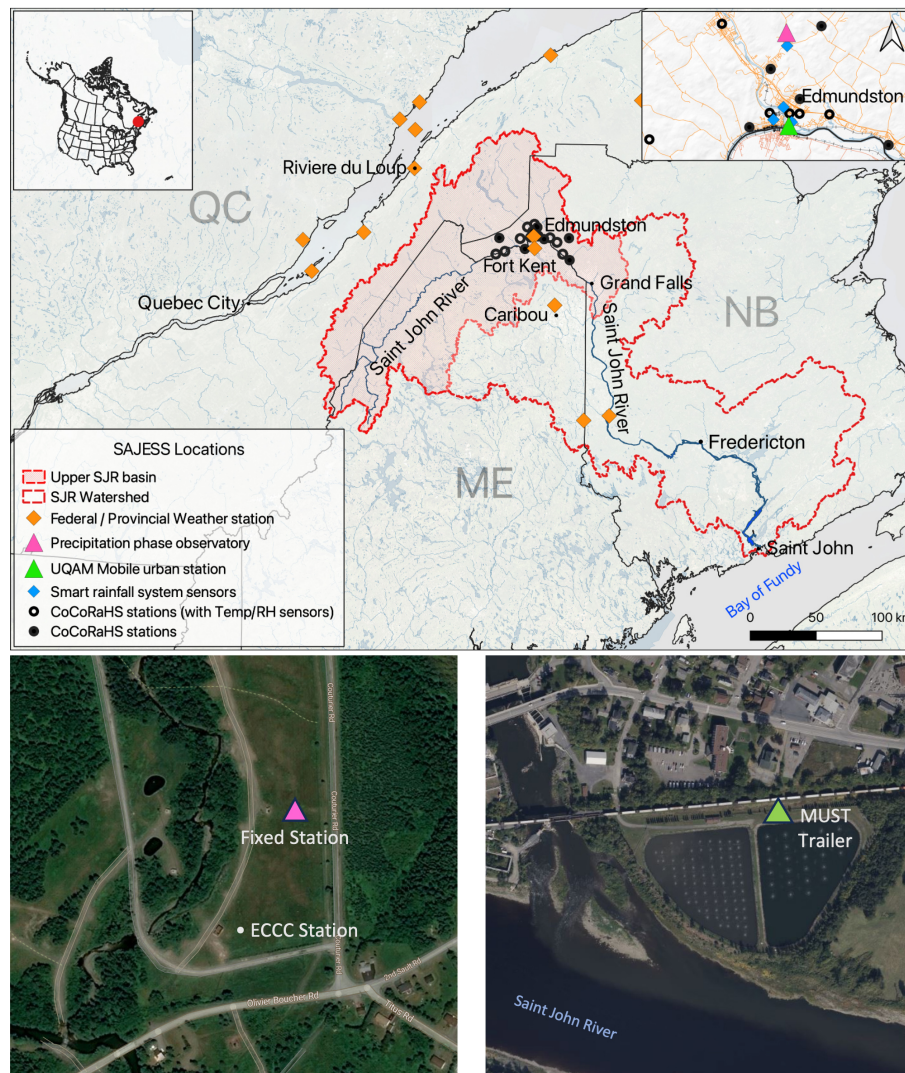


**Figure 1.** Top: the upper Saint John River basin (shaded red), straddling the borders of Quebec (QC), Maine (ME, United States), and New Brunswick (NB) is a sub-basin of the Saint John River basin (red line). The Environment and Climate Change Canada (ECCC) and US National Weather Service (NWS) weather stations, SAJESS-supplied CoCoRaHS stations including where temperature–RH sensors were also co-located (black circles), the precipitation phase observatory/Fixed Station (pink triangle), and the UQAM MUST Trailer (green triangle) are shown. Bottom: aerial photographs of the two main SAJESS sites showing the locations of the Fixed Station, MUST Trailer, and ECCC station. © Microsoft product screenshots reprinted with permission from © Microsoft Corporation.

cations for either a satellite dish associated with the Smart Rainfall System (SRS) array (Colli et al., 2019) or a precipitation gauge and snow board for the Community Collaborative Rain, Hail, and Snow Network (CoCoRaHS) (Cifelli et al., 2005). Furthermore, 10 grade 6 classes (11–12 years old) from local elementary schools also enrolled as CoCoRaHS observers.

## 2.2 Precipitation phase observatory

The precipitation phase observatory (henceforth the Fixed Station) encompassed a semi-permanent array of meteorological instruments that were installed  $\sim 100$  m from the Ed-

mundston ECCC station on 30 November 2020 (Table 1, Figs. 1 and 2). The site was situated at the southern end of an area of open grassland in a broad valley, 152 m above sea level (a.s.l.). The valley is 120–200 m wide by 1 km long, oriented north–south, and bordered by coniferous forest. The 14 ha site acts as the municipal aquifer resupply and was provided by the City of Edmundston for the installation. We provide specific location details in Table 1. This site was chosen to allow for the SAJESS datasets to be supplemented and compared with records from the nearby ECCC station, which was comprised of a Geonor T-200B weighing precipitation gauge with a single Alter shield, three sonic ranger snow depth sensors, three temperature–RH probes, and a RM

Young wind monitor atop a 10 m mast. Additionally, the open field provided an opportunity to install an infrared gas analyzer and sonic anemometer (IRGASON) to estimate surface turbulent fluxes and compute surface energy balances (Table 2) during the IOP (see Sect. 2.2).

The identification of precipitation phase was achieved at the Fixed Station by the installation of a laser-optical disdrometer for recording particle size and fall speed and by a vertically pointing micro rain radar (MRR) to provide information on the atmospheric conditions aloft (see Sect. 3 and Table 2). A K63 Hotplate Total Precipitation Gauge (henceforth hotplate) was installed to measure precipitation rate and amount. Aside from periods of missing data ( $\sim 5\%$ ), the Fixed Station dataset, excluding the flux tripod (see Sect. 3.1.2), spans 1 December 2020–30 April 2021.

### 2.3 Intensive observation period

Due to limitations at the Fixed Station (e.g., no fuel or generator use), a separate IOP site was established so that the Mobile Urban Weather Station (MUST) Trailer and instruments could frequently be visited by observers (Fig. 1). The 6 ft  $\times$  12 ft enclosed trailer was equipped with heating, AC power, helium cylinders, and instrument storage; it was parked on a fenced parcel of land on the north bank of the Saint John River and the east bank of the mouth of the Madawaska River, 143 m a.s.l. Although the 3.3 ha site is dominated by the Edmundston wastewater ponds, there was sufficient space for the MUST Trailer and instrumentation to be placed along the northern edge of the site (Fig. 4).

The proximity of the instruments to the open ponds, nearby railway, and urban environment resulted in the focus on manual observations of weather conditions and precipitation type, rather than automated instrumentation, at this location. We therefore stationed equipment that required regular attention or manual operation, such as the multi-angle snowflake camera (MASC) (Fig. 3c) and macrophotography equipment (not shown). Manual observations and macrophotography (see Sect. 3.2) were conducted at the site from 1 March 2021–27 April 2021.

### 2.4 Smart Rainfall System (SRS)

The Smart Rainfall System (SRS) was installed at six sites in the Edmundston area to capture the spatial variability of precipitation by exploiting the satellite-to-earth links' technology (Colli et al., 2019). Some locations were also chosen to provide measurements upstream and downstream of Edmundston. The SRS uses a standard parabolic dish to receive satellite telecommunication broadcasting signals, and an algorithm converts the signal attenuation to precipitation rate (Sect. 3.4). Locations with parabolic dishes that were already installed by community volunteers for telecommunication purposes, but not used during the experiment period, were selected. Locations are shown in Fig. 1.

### 2.5 Community involvement (CoCoRaHS)

While the CoCoRaHS network provides a broad array of precipitation measurements across North America (Reges et al., 2016), there were few CoCoRaHS observer sites in the SAJESS study region. With assistance from CoCoRaHS Canada (Colorado Climate Center, 2017), SAJESS students and staff facilitated the distribution of equipment and training to a total of 21 new CoCoRaHS stations (Table 4), including 10 elementary schools, during the 2020–2021 winter season. CoCoRaHS site metadata available to the public can be found at <https://cocorahs.org/Stations/ListStations.aspx> (last access: 5 December 2023).

## 3 Field instruments and manual observations

### 3.1 Instrumentation

The main consideration when deploying instruments to SAJESS was how to measure the amount, phase, and type of precipitation that occurs during the winter and spring seasons. Particular attention was paid to gathering data throughout as much of the tropospheric column as possible.

Here we provide an overview of the instrumentation used during SAJESS. Sensor details, parameters, and units are included in Tables 2 and 3. Further details of each sensor, such as the date of manufacture, last calibration, and serial number, are also provided in the README files.

#### 3.1.1 Meteorological tripod

Standard meteorological variables were measured at each of the two main sites. Common parameters for each site were 2 m air temperature and relative humidity, four-way net radiation (upwelling and downwelling long-wave and short-wave radiation, LW $\uparrow$ , LW $\downarrow$ , SW $\uparrow$ , and SW $\downarrow$ ), surface temperature, and snow depth. Measurements at the Fixed Station also included soil surface temperature and moisture content. Snow at the Fixed Station remained undisturbed for the winter, and total snow depth was recorded continuously for December 2020–April 2021. Due to disturbance of the snowpack surrounding the MUST Trailer by foot traffic, vehicles, and the installation of other instruments, a 30 cm  $\times$  30 cm white snow board was placed underneath the snow depth sensor and cleared after each significant snowfall event. The clearing of the snow boards was consistently performed by the volunteers/students. They were cleared at the beginning of observations before precipitation started and then cleared again once precipitation ended. Through these actions, the ensuing data should be considered by users as a snowfall measurement rather than true snow depth. On each meteorological tripod, the snow depth sensor was installed on the south end of the tripod cross arm so that the legs of the tripod would not be within  $\sim 1$  m diameter cone of detection. For surface temperature, two infrared radiometers (IRRs; henceforth IRR 1 and IRR 2) were mounted to the north end of

**Table 1.** Primary site information.

| Location      | Lat. (° N) | Long. (° W) | Elevation (m) | Surface                      | Surroundings   | Dates of operation for SAJESS |
|---------------|------------|-------------|---------------|------------------------------|--|-------------------------------|
| Fixed Station | 47.418     | 68.324      | 152           | Grassland on gravel riverbed | Open grassland in broad river valley, rural road ~ 150 m to the west   | 1 December 2020–30 April 2021 |
| MUST Trailer  | 47.361     | 68.320      | 143           | Packed gravel, short grass   | Site on edge of city treatment ponds, ~ 250 m from confluence of two large rivers; suburban subdivision to the north | 1 March 2021–30 April 2021    |

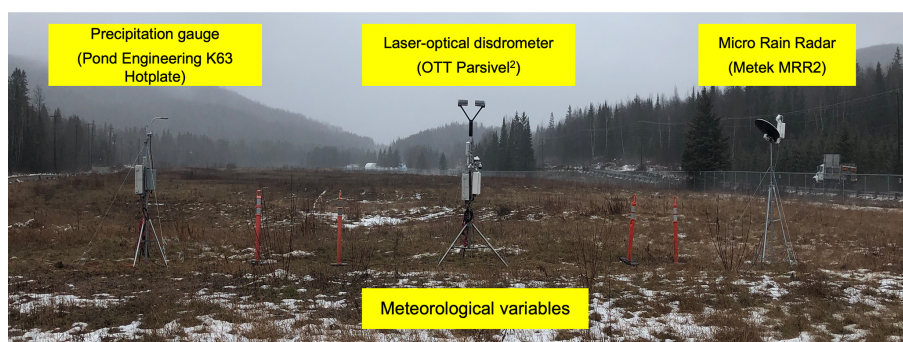


**Figure 2.** The precipitation phase observatory instrumentation, image taken looking north. From left-to-right: the K63 Hotplate, a laser-optical disdrometer installed upon the meteorological tripod, and the micro rain radar. This station was also to be known as the “Fixed Station”. Picture taken 1 December 2020.

the cross arm of each meteorological tripod and angled away ~ 30°. At the Fixed Station, IRR 1 faced slightly west, while IRR 2 faced slightly east. At the MUST Trailer site, these were reversed. The net radiometer and snow depth sensors were mounted on the south end of each cross arm.

### 3.1.2 Flux tripod

An open-path eddy-covariance system was installed at the Fixed Station for the IOP from 5 March 2021 to 30 April 2021. The integrated infrared gas analyzer and sonic anemometer (IRGASON), temperature–RH probe, net radiometer, infrared radiometer, soil probes, and heat flux plates were installed following the prescribed methods found in Campbell Scientific (2022a), with the IRGASON sensor facing north into the prevailing wind. Winds (in 3-D), air temperature, ambient pressure, and CO<sub>2</sub> and H<sub>2</sub>O densities were captured at 10 Hz resolution and averaged over 30 min to calculate turbulent fluxes and energy closure balances (Campbell Scientific, 2022b). The dataset also includes diagnostic data, data quality values, and coefficients used for the eddy-covariance calculations during each 30 min period so the raw time series data can also be post-processed using a variety of software (US Department of Energy, 2021).

### 3.1.3 Hotplate precipitation gauge

A hotplate precipitation gauge (henceforth hotplate) was installed at the eastern end of the Fixed Station instrument array (Fig. 3) (Rasmussen et al., 2011; Thériault et al., 2021b). As outlined by Cauteruccio et al. (2021), the hotplate was tested during the World Meteorological Organization’s Solid Precipitation Intercomparison Experiment (SPICE) (Nitu et al., 2018) and the Global Precipitation Measurement Cold Season Precipitation Experiment (GCPEX) (Skofronick-Jackson et al., 2015). The hotplate measures liquid-equivalent precipitation by recording 1 and 5 min running averages of precipitation rate and wind speed (needed as control for precipitation rate). An accompanying environmental sensor measures air temperature, RH, and atmospheric pressure with the same 1 and 5 min temporal resolution. SAJESS was the first time in Canada that the Pond Engineering version of the hotplate was used in a field campaign (Pond Engineering, 2021). A second one of this type of hotplate was installed for the IOP on the MUST Trailer mast and is detailed in Sect. 3.1.7.

### 3.1.4 Disdrometer

A laser-optical disdrometer was deployed at the Fixed Station for the duration of the field campaign on the same tri-

**Table 2.** Instrument details for the SAJESS Fixed Station site.

| Installation (instrument abbr.) | Instrument  | Installation height    | Variable   | Units  | Resolution  | Accuracy  |
|---------------------------------|---|------------------------|--|--|---|---|
| Meteorological tripod (MET)     | Campbell Scientific CR1000X data logger           | 1.5 m                  | Data recording   | n/a  | n/a   | n/a   |
|                                 | OTT Parsivel <sup>2</sup> disdrometer             | 2.80 m                 | Timestamp<br>Intensity of precipitation ( $\text{mm h}^{-1}$ )<br>Precipitation since start (mm)<br>Weather code SYNOP WaWa<br>Weather code METAR/SPECI<br>Weather code NWS<br>Radar reflectivity (dBZ)<br>MOR visibility (m)<br>Signal amplitude of laser band<br>Number of detected particles<br>Temperature in sensor ( $^{\circ}\text{C}$ )<br>Heating current (A)<br>Sensor voltage (V)<br>Kinetic energy<br>Snow intensity ( $\text{mm h}^{-1}$ )<br>V0D0 ... V31D31 | Timestamp<br>$\text{mm h}^{-1}$<br>Mm<br>val<br>val<br>val<br>dBZ<br>m<br>val<br>val<br>$^{\circ}\text{C}$<br>A<br>V<br>$\text{J (m}^2 \text{ h)}^{-1}$<br>$\text{mm h}^{-1}$<br>val | 1 min (average), except for the VxDx size and fall speed classes, which represent a 1 min sum | Accuracy is not given by OTT for the individual variables; however the size classification is given by OTT $\pm 1$ size class (0.2 to 2 mm) $\pm 0.5$ size class (>2 mm)        |
|                                 | Vaisala HMP155 temperature–RH probe               | 2.00 m                 | Air temperature<br>Relative humidity   | $^{\circ}\text{C}$<br>%  | 1 min (average)   | $0.226 + 0.0028 \times \text{reading} (-80 \text{ to } +20^{\circ}\text{C})$<br>$0.055 + 0.0057 \times \text{reading} (+20 \text{ to } +60^{\circ}\text{C})$                    |
|                                 | Kipp & Zonen CNR4 net radiometer                  | 1.80 m                 | Four-way net radiation   | $\text{W m}^{-2}$  | 1 min (average)   | <5 %  |
|                                 | Campbell Scientific SR50A sonic ranger            | 1.80 m                 | Snow depth   | m  | 1 min (average)   | $\pm 1$ cm  |
|                                 | Apogee SI-411 IR radiometer                       | 1.80 m                 | Surface temperature  | $^{\circ}\text{C}$   | 1 min (average)   | $\pm 0.2^{\circ}\text{C}$   |
|                                 | Campbell Scientific CS655 Soil probe (vertically) | 0.00 m                 | Soil temperature<br>Soil moisture content<br>Soil electrical conductivity  | $^{\circ}\text{C}$<br>%<br>$\text{dS m}^{-1}$  | 1 min (average)   | $\pm 0.1\text{--}0.5^{\circ}\text{C}$<br>$\pm 1\% \text{--}3\%$<br>$\pm 5\%$ of reading<br>$+0.05 \text{ dS m}^{-1}$  |
| MRR tripod (MRR)                | METEK MRR-2                                       | 2.60 m                 | Doppler raw spectra<br>Reflectivity (Ze)<br>Doppler velocity (W)<br>Spectral width ( $\sigma$ )  | dB<br>dBZ<br>$\text{m s}^{-1}$<br>$\text{m s}^{-1}$  | 10 s raw data; 1 min average; see Sect. 3.1.5   | 0.53 dB<br>0.53 dBZ<br>$0.109 \text{ m s}^{-1}$<br>$0.09 \text{ m s}^{-1}$  |
| Hotplate tripod (HP)            | Pond Engineering K63 Hotplate precipitation gauge | 2.60 m                 | Air temperature<br>Barometric pressure<br>Precipitation rate<br>Accumulation<br>Wind speed<br>Hotplate power   | $^{\circ}\text{C}$<br>kPa<br>$\text{mm h}^{-1}$<br>mm<br>$\text{m s}^{-1}$<br>W  | 1 min (average)<br>5 min (average)  | $\pm 1^{\circ}\text{C}$<br>$\pm 1$ kPa<br>$\pm 0.5 \text{ mm h}^{-1}$<br>$\pm 0.5$ mm<br>$\pm 1 \text{ m s}^{-1}$<br>n/a  |
| Flux tripod (FLUX)              | Campbell Scientific CR1000X data logger           | 1.5 m                  | Data recording   | n/a  | n/a   | n/a   |
|                                 | Vaisala HMP155 temperature–RH probe               | 2.00 m                 | Air temperature<br>Relative humidity   | $^{\circ}\text{C}$<br>%  | 30 min (average)  | $0.226 + 0.0028 \times \text{reading} (-80 \text{ to } +20^{\circ}\text{C})$<br>$0.055 + 0.0057 \times \text{reading} (+20 \text{ to } +60^{\circ}\text{C})$                    |
|                                 | Apogee SI-411 IR radiometer                       | 1.80 m                 | Surface temperature  | $^{\circ}\text{C}$   | 30 min (average)  | $\pm 0.2^{\circ}\text{C}$   |
|                                 | Kipp & Zonen CNR4 Net radiometer                  | 1.80 m                 | Four-way net radiation   | $\text{W m}^{-2}$  | 30 min (average)  | <5 %  |
|                                 | Campbell Scientific IRGASON                       | 2.00 m                 | 3D wind<br>CO <sub>2</sub> density<br>H <sub>2</sub> O density<br>Sonic temperature  | $\text{m s}^{-1}$<br>$\text{mg m}^{-3}$<br>$\text{g m}^{-3}$<br>$^{\circ}\text{C}$   | 10 Hz   | $1 \text{ mm s}^{-1}$<br>$0.2 \text{ mg m}^{-3}$<br>$(0.15 \mu\text{mol mol}^{-1})$<br>$0.00350 \text{ g m}^{-3}$<br>$(0.006 \text{ mmol mol}^{-1})$<br>$0.025^{\circ}\text{C}$ |
|                                 | Campbell Scientific CS655 Soil probe              | 2.5 cm (below surface) | Soil temperature<br>Soil moisture content<br>Soil electrical conductivity  | $^{\circ}\text{C}$<br>%<br>$\text{dS m}^{-1}$  | 30 min (average)  | $\pm 0.1\text{--}0.5^{\circ}\text{C}$<br>$\pm 1\% \text{--}3\%$<br>$\pm 5\%$ of reading<br>$+0.05 \text{ dS m}^{-1}$  |
|                                 | Campbell Scientific HFP01 Soil heat flux plates   | 8 cm (below surface)   | Soil heat flux   | $\text{W m}^{-2}$  | 30 min (average)  | $-15\%$ to $+5\%$ in most common soils  |

n/a: not applicable.

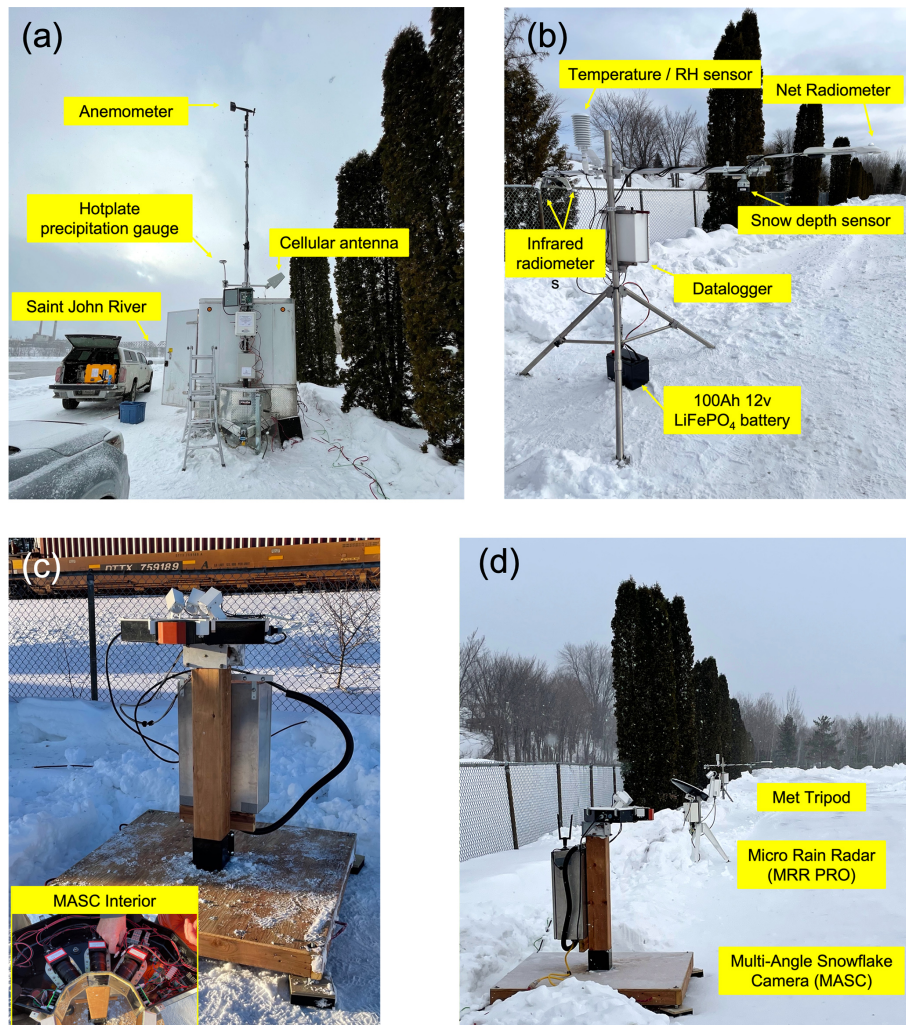


**Figure 3.** Instruments and sensors co-located with the Mobile Urban Weather Station (MUST) Trailer. (a) The MUST Trailer with extended 10 m mast, anemometer (not included in the dataset), and K63 Hotplate; (b) the meteorological tripod; (c) the multi-angle snow camera (MASC) with a top-down view of the internal components and three high-speed cameras; and (d) the MASC, MRR-Pro, and meteorological tripod lined along the access road to the water treatment lagoon. Pictures taken 3 March 2021.

pod as the standard meteorological instruments, at 2.8 m above ground level (a.g.l.) (Fig. 3). The disdrometer provides measurements of the size and speed of falling hydrometeors which, when post-processed accordingly, can provide a classification of hydrometeor type (Hauser et al., 1984; Rasmussen et al., 1999; Löffler-Mang and Joss, 2000; Ishizaka et al., 2013; Thériault et al., 2021a). Included in the dataset are variables derived by the manufacturer’s software such as precipitation intensity ( $\text{mm h}^{-1}$ ), number of detected particles, and several national standard present weather codes. The spectrum of particles is provided by 1024 columns representing the  $32 \times 32$  matrix of particle fall speed and diameter bins. The mid-values and spread of these bins are listed in the README file supplied with the dataset and in the disdrometer user manual (OTT, 2019).

### 3.1.5 Micro rain radar

A micro rain radar (MRR) at each of the primary sites was used during SAJESS to vertically profile hydrometeor reflectivity and Doppler velocity (Tokay et al., 2009; Souverijns et al., 2017). A METEK MRR-2 was installed at the Fixed Station, 2.6 m a.g.l., at the western end of the instrument array (Fig. 3). The MRR-2 has 32 range gates (height steps), and we set the height resolution to the maximum of 200 m, giving a maximum height of 6400 m. Raw data from the MRR-2 were post-processed using the IMProToo algorithm from Maahn and Kollias (2012), as outlined in Thériault et al. (2021a). An MRR-Pro was installed at 1.3 m a.g.l. at the MUST Trailer (Fig. 4d). Settings for the MRR-Pro were 128 range gates, 64 spectral lines, 10 s sampling, 50 m height resolution, and 6350 m ceiling. The combination of these pa-

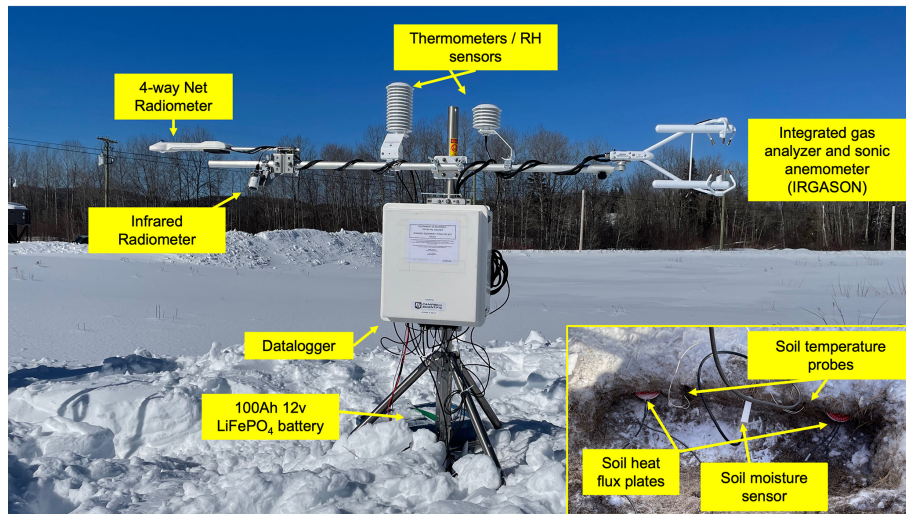


**Figure 4.** The Fixed Station flux tripod. An open-path eddy-covariance system consisting of an infrared gas analyzer and sonic anemometer (IRGASON), soil temperature probes, a soil moisture sensor, a net radiometer, an infrared radiometer, and temperature–RH sensors. This tripod was installed for the melt period from 5 March to 30 April 2021. Picture taken 5 March 2021.

rameters results in a velocity range of  $12 \text{ m s}^{-1}$  and a velocity resolution of  $0.19 \text{ m s}^{-1}$ . The 10 s averaging time results in a total of 305 spectra being averaged for each measurement. Both radar units used built-in dish heating to eliminate snow and ice build-up during precipitation events.

### 3.1.6 Multi-angle snowflake camera

A multi-angle snowflake camera (MASC) was installed at the MUST Trailer (Fig. 4c and d), on a wooden stand  $\sim 1.4 \text{ m}$  above the ground, for the majority of the IOP (5 March 2021–27 April 2021). Accumulating snow around the base of the stand was removed by students to prevent the re-suspension of previously captured particles (Fitch et al., 2021; Schaer et al., 2020). The MASC consists of three high-speed cameras housed in a single enclosure, with  $36^\circ$  separation between each camera, and a focal point  $\sim 10 \text{ cm}$  for each lens. The cameras take images simultaneously when particles are detected within a ring-shaped viewing area (Fig. 4c inset). The three images from each trigger consequently show the hydrometeor(s) from slightly different angles. First introduced by Garret et al. (2012), MASCs have been deployed in Antarctica (Praz et al., 2017), the Colorado Rockies (Hicks and Notaroš, 2019), and Alaska (Fitch et al., 2021). Images have been used individually to illustrate the hydrometeors observed and highlight the riming conditions, crystal habit, and size of particles.

### 3.1.7 MUST Trailer mast

A telescopic pneumatic 10 m mast attached to the MUST Trailer supported an anemometer and wind vane (at 10 m), a hotplate precipitation gauge at 3.5 m, and the antenna for

upper-air observations (see Sect. 3.3) (Fig. 4a). Due to air leakage, the mast did not always maintain its full extension and therefore required re-extending at times. This, in addition to the proximity of the trailer to trees and a nearby structure, has resulted in us excluding the wind data from the publicly available dataset.

## 3.2 Macrophotography, manual observations, and time lapse images

Observers were present at the MUST Trailer during periods of precipitation to report weather conditions and to obtain macrophotographs of solid hydrometeors (Gibson and Stewart, 2007; Joe et al., 2014; Thériault et al., 2018; Thériault et al., 2021a). This provided a running record of the weather conditions during storm events and allowed for the field training of students in manual observations and identification of precipitation types and snow crystal habits. The recording of manual observations can also remove doubt about precipitation arriving at the surface. This is especially important with respect to hydrometeor type during periods of near-freezing conditions, during which a mixture or changes in precipitation phase or type can occur. This also reduces the potential for misdiagnosis by instrumentation or modelling. Observations of sky condition, cloud type, and precipitation type (solid, liquid, or mixed), and images from a digital single-lens reflex (SLR) camera fitted with a macro lens and ring flash, were taken every 10 min. Precipitation was collected on a black velvet collection pad during a short period (5–30 s), depending on the precipitation rate. The aim was to ensure that there were enough particles to represent the precipitation conditions, while avoiding particles overlapping each other. The collection pad was wiped ev-



**Table 3.** Instrument details for the SAJESS MUST Trailer site.

| Installation (instrument abbr.) | Instrument   | Installation height | Variable  | Units   | Resolution      | Accuracy   |
|---------------------------------|--|---------------------|---|---|-----------------|--|
| Meteorological tripod (MET)     | Campbell Scientific CR1000X data logger                            | 1.5 m               | Data recording  | n/a   | n/a             | n/a  |
|                                 | Vaisala HMP155 temperature–RH probe                                | 2.00 m              | Air temperature<br>Relative humidity  | °C<br>%   | 1 min (average) | 0.226 + 0.0028 × reading<br>(−80 to +20 °C)<br>0.055 + 0.0057 × reading<br>(+20 to +60 °C) |
|                                 | Kipp & Zonen CNR4 net radiometer                                   | 1.80 m              | Net four-way radiation  | W m <sup>−2</sup>                                   | 1 min (average) | <5 %   |
| 10 m mast (MAST)                | Campbell Scientific SR50A  | 1.80 m              | Snow depth  | m   | 1 min (average) | ±1 cm  |
|                                 | Campbell Scientific CR1000X data logger                            | 1.5 m               | Data recording  | n/a   | n/a             | n/a  |
| MASC Platform (MASC)            | Pond Engineering K63 Hotplate precipitation gauge                  | 2.60 m              | Air temperature   | °C  | 1 min (average) | ±1 °C  |
|                                 |  |                     | Barometric pressure   | kPa   | 5 min (average) | ±1 kPa   |
|                                 |  |                     | Precipitation rate  | mm h <sup>−1</sup>                                  |                 | ±0.5 mm h <sup>−1</sup>  |
|                                 |  |                     | Accumulation  | mm  |                 | ±0.5 mm  |
|                                 |  |                     | Wind speed  | m s <sup>−1</sup>                                   |                 | ±1 m s <sup>−1</sup>   |
|                                 |  |                     | Hotplate power  | W   |                 | n/a  |
| MASC Platform (MASC)            | Multi-angle snowflake camera                                       | 1.00 m              | Series of three images  | n/a   | Up to 3 Hz      | n/a  |
| MRR-Pro (MRR)                   | METEK MRR-Pro  | 1.30 m              | Doppler raw spectra<br>Reflectivity ( <i>Z</i> <sub>e</sub> )<br>Doppler velocity ( <i>W</i> )<br>Spectral width ( <i>σ</i> ) | dB<br>dBZ<br>m s <sup>−1</sup><br>m s <sup>−1</sup> | see Sect. 3.1.5 | 0.53 dB<br>0.53 dBZ<br>0.109 m s <sup>−1</sup><br>0.09 m s <sup>−1</sup>                   |
| Macrophotography (MP)           | Nikon D80 with 60 mm macro lens                                    | n/a                 | Series of nine images   | n/a   | 10 min          | n/a  |
| Manual observations (OBS)       | Volunteer and/or student   | n/a                 | Sky condition<br>Cloud type<br>Precipitation type<br>Blowing snow<br>Light precipitation                                      | Oktas<br>Type<br>Type<br>Yes/no<br>Yes/no           | 10 min          | n/a  |
| Upper-air observations (SB)     | iMet-3050A 403 MHz portable sounding system with iMet-4 radiosonde | n/a                 | Air temperature<br>Relative humidity<br>Wind speed<br>Wind direction<br>Pressure<br>Geopotential height                       | °C<br>%<br>m s <sup>−1</sup><br>degrees<br>hPa<br>m | 1 s             | ±0.5–1.0 °C<br>±5 %<br>±0.5 m s <sup>−1</sup><br>±1°<br>±0.5–2.0 hPa<br>±15 m              |

n/a: not applicable.

ery time after the series of nine images were taken using a set sequence of movements of the camera upon a sliding frame. Images of a ruler placed across the pad for scale were taken intermittently, for example when the camera was removed/replaced on the stand. Users can assume the scale remains constant between these images (each image is 2 cm across). The scale images are listed in the macrophotography README file. More details of the method, including images of the equipment, can be found in Thériault et al. (2021a) and (2018). Other conditions to note were the occurrence of very light precipitation which can be missed by disdrometers and the presence of blowing snow that could affect analysis of MASC data (Sect. 3.1.6).

Hourly images of each site, including the surface conditions around the instruments, were captured by a time lapse camera. Similar previous campaigns by the authors have found time lapse images to be very useful in confirming sky

and surface conditions such as snow-on-the-ground onset, and they have also provided evidence of wildlife encounters with the instrumentation. Precipitation-type diagnoses, however, are not usually possible with these images.

### 3.3 Upper-air observations

Soundings were timed to coincide with the standard synoptic times of 00:00, 03:00, 06:00, 09:00, 12:00, 15:00, 18:00, or 21:00 UTC. Some additional launches were attempted to coincide with precipitation phase transitions. Sonde retrieval was not attempted during this experiment. A total of 52 balloons were launched from the MUST Trailer, and we include text files for 46 of those launches that resulted in a complete sounding of the troposphere from which profiles of pressure, temperature, dew point, and winds (speed and direction) can be produced. Files of each sounding are also available from the authors in other commonly used sounding formats.

**Table 4.** Locations of CoCoRaHS stations founded during SAJESS, with HOBO MX2301A temperature–RH information (if present).

| CoCoRaHS ID | Temp–RH sensor ID (if present) | Lat. (° N) | Long. (° W) | Elevation (m) | Temp–RH sensor period of record |
|-------------|--------------------------------|------------|-------------|---------------|---------------------------------|
| CAN-NB-111  | SJ_HOBOTEMP_01                 | 47.37      | 68.32       | 166           | 11 December 2020–30 April 2021  |
| CAN-NB-112  | Not present                    | 47.35      | 68.67       | 198           |                                 |
| CAN-NB-113  | SJ_HOBOTEMP_02                 | 47.25      | 68.03       | 155           | 11 December 2020–30 April 2021  |
| CAN-NB-114  | SJ_HOBOTEMP_03                 | 47.37      | 68.31       | 197           | 10 December 2020–30 April 2021  |
| CAN-NB-115  | SJ_HOBOTEMP_04                 | 47.43      | 68.39       | 142           | 10 December 2020–30 April 2021  |
| CAN-NB-117  | SJ_HOBOTEMP_05                 | 47.45      | 68.32       | 326           | 11 December 2020–30 April 2021  |
| CAN-NB-121  | Not present                    | 47.21      | 67.96       | 154           |                                 |
| CAN-NB-122  | Not present                    | 47.40      | 68.34       | 144           |                                 |
| CAN-NB-126  | Not present                    | 47.38      | 68.31       | 192           |                                 |
| CAN-NB-127  | SJ_HOBOTEMP_06                 | 47.36      | 68.16       | 176           | 5 March 2021–30 April 2021      |
| CAN-NB-133  | SJ_HOBOTEMP_07                 | 47.35      | 68.46       | 332           | 5 March 2021–30 April 2021      |
| CAN-NB-134  | Not present                    | 47.28      | 68.41       | 155           |                                 |
| CAN-NB-135  | SJ_HOBOTEMP_08                 | 47.26      | 68.61       | 167           | 12 December 2020–30 April 2021  |
| CAN-NB-139  | SJ_HOBOTEMP_09                 | 47.37      | 68.34       | 241           | 10 December 2020–30 April 2021  |
| CAN-NB-140  | Not present                    | 47.36      | 67.97       | 295           |                                 |
| CAN-NB-141  | Not present                    | 47.43      | 68.29       | 348           |                                 |
| CAN-NB-142  | Not present                    | 47.36      | 68.36       | 189           |                                 |
| CAN-NB-143  | SJ_HOBOTEMP_10                 | 47.24      | 68.70       | 170           | 12 December 2020–30 April 2021  |
| CAN-NB-144  | SJ_HOBOTEMP_11                 | 47.37      | 68.28       | 141           | 10 December 2020–30 April 2021  |
| CAN-NB-145  | SJ_HOBOTEMP_12                 | 47.33      | 68.09       | 231           | 5 March 2021–30 April 2021      |
| CAN-NB-147  | Not present                    | 47.35      | 68.22       | 164           |                                 |
| n/a         | SJ_HOBOTEMP_13                 | 47.29      | 68.39       | 156           | 5 March 2021–30 April 2021      |

n/a: not applicable.

### 3.4 Smart Rainfall System

SAJESS served as the opportunity to deploy an innovative environmental monitoring technique, the Smart Rainfall System (SRS), that has been developed by the University of Genoa, Genoa, Italy, and currently distributed by Artys srl. The SRS produces estimations of liquid precipitation, in 1 min rainfall intensity, by processing the attenuation of the satellite microwave link (SML) signal emitted by commercial geosynchronous satellites for Digital Video Broadcasting (DVB-S) and received by common parabolic antennas (Colli et al., 2020). Estimating liquid precipitation using the SRS has been confirmed by several experimental initiatives (Giannetti and Reggiannini, 2021). In contrast, snowfall intensity retrieval at centimetre wavelengths (the DVB-S signal is transmitted in the Ku frequency band) is more uncertain. It has been demonstrated that higher operating frequencies, and preferably dual-band systems, are needed to successfully retrieve solid precipitation (Falconi et al., 2018; Liao et al., 2016).

SAJESS provided the experimental conditions for SRS devices to monitor the liquid content in cases of mixed precipitation and wet (melting) snow. The SRS tested in Edmundston was composed of a set of distributed SML sensors, as described by Colli et al. (2019), connected to a central processing and analysis node to reconstruct the bi-dimensional rainfall field in real time. To an onlooker, the only equipment visible is a small box placed inside the residence that con-

nects inline to the satellite dish coaxial cable. The processor inside the box is then configured to connect to the local wi-fi network. To reduce signal noise, it is preferable that the satellite dish no longer be in service. These results will be published once work is complete.

### 3.5 CoCoRaHS sites

#### 3.5.1 CoCoRaHS gauges and snow boards

Volunteers from the community and local elementary schools contributed to SAJESS by recording meteorological measurements for the CoCoRaHS network (Cifelli et al., 2005). This provided an opportunity for students to engage in the data collection process and to learn about the importance (and difficulties) of precipitation determination. A typical CoCoRaHS station includes a manual precipitation gauge to measure liquid and solid precipitation and a 40 cm × 40 cm white board for measuring snow depth. Daily measurements include the amount of precipitation, depth of snowfall, and snow water equivalent (SWE). Weekly measurements consist of total snow depth and the total SWE. CoCoRaHS data can be found using the network's online database; station details are provided in Table 4. In addition to the regular CoCoRaHS station equipment, some volunteers hosted data loggers to record air temperature and relative humidity (see below).

### 3.5.2 Temperature sensors

HOBO MX2301A data loggers were distributed to 13 community volunteers (Fig. 1, Table 4), and correct installation of each sensor was confirmed by a SAJESS team member. Installed approximately 2 m a.g.l., the data loggers measure air temperature and relative humidity every 5 min (Onset Computer Corporation, 2022). These low-cost, robust sensors provided a broad (50–60 km) network to assess spatial variability in near-surface temperature–RH, especially during the passage of fronts and the onset/cessation of precipitation. Data were retrieved from the HOBO devices via a Bluetooth smartphone app that reduced the need to handle the sensor.

## 4 Data description

### 4.1 Data processing and management

Here we provide a short summary of the data processing and archiving strategies. Full details on all data, including specifications of the instruments used, can be found in the README files uploaded to the Federated Research Data Repository (FRDR).

Firstly, all instrumentation, camera equipment, observer notes, and computers were set to UTC date and time. Instruments that produce relatively low-volume text-based data, such as the disdrometer, meteorological tripods, hotplate precipitation gauge, and temperature sensors, have been processed by concatenating smaller files together to create monthly files. Missing timestamps have been added to ensure every file contains time steps for each minute of the month. All missing data points have been filled with NaNs, and no interpolation of missing data points has been attempted for the data uploaded to the FRDR. For standard meteorological variables, such as temperature, humidity, snow depth, and radiation measurements, values have been quality checked to ensure they fall within the operating range of each instrument, with values outside of these ranges being set to NaN.

Raw radar data (.raw files) from the Fixed Station radar have been processed into daily NetCDF (.nc) format using the algorithm detailed by Maahn and Kollias (2012). Both .raw and .nc files have been included in this dataset. Hourly data from the MUST Trailer radar (MRR-Pro) have been archived as .nc files as these data are produced by the instruments embedded processor (METEK, 2017)

Photographic images have not been altered or cropped and are uploaded as .png files for the MASC and macrophotography or .jpg files for the time lapse cameras. Manual observations recorded in spreadsheets have been archived as comma-separated-value (.csv) files. Upper-air observations are saved as one file per sounding, in tabular-delimited files, indexed by UTC date and time at a temporal resolution of 1 s.

In most instances, files have been identified using a specific naming convention using abbreviations for the

project (SAJESS, SJ), each site (Fixed Station, FS; MUST Trailer, MT), and each instrument (see Tables 2 and 3). For example, data from the disdrometer at the Fixed Station for the month of January 2021 are contained in the file SJ\_FS\_DIS\_MAS\_202112.txt. (The abbreviation MAS stands for master and is used by the field staff to identify data that have been assembled ready for upload to the repository.) MASC images do not follow this naming convention as the software used with the instrument provides a detailed filename with respect to the snowflake number and timestamp of the image.

### 4.2 Data validity

While not exhaustive, below we list known issues and attempts to date at validating data from the SAJESS instruments and observations. To preserve the raw data recorded during SAJESS, no quality-control-related post-processing has been performed. We encourage all users to perform quality control and post-processing according to their needs. We invite users to contact us for further information as several projects using SAJESS data are ongoing.

#### 4.2.1 Meteorological tripod

To our knowledge, the only instrument to suffer from a systematic error was the HMP155A temperature and humidity probe located on the meteorological tripod at the Fixed Station. Incomplete grounding at the data logger, and the subsequent data logger program, resulted in a bias of  $\sim -2.32^\circ\text{C}$  when compared to temperature data from the ECCC station (Fig. 5). Due to the uniform pattern of the bias resulting in a low RMSE, these data have been retained in the dataset and are available for use. Correction of these data by  $+2.32^\circ\text{C}$  in ongoing snow modelling analyses indicates these data are still useful if post-processed accordingly. Post-deployment testing indicates that this bias is not present in the temperature data from the MUST Trailer meteorological tripod.

While data from the hotplate precipitation gauge include air temperature and humidity that align well with the ECCC station (i.e., do not require bias correction), these data have significantly more noise than data from the meteorological tripod sensor.

Analysis of the IRR surface temperature data indicates that shading from the tripod and data logger enclosure may have affected these measurements. When snow was present, the side with a shaded field of view (west in the morning and east in the evening) measured warmer conditions (up to  $\sim 2^\circ\text{C}$ ) than on the unshaded side. Once snow cover was absent, the trend was reversed so that the shaded side is cooler (up to  $\sim 6^\circ\text{C}$ ). This diurnal pattern of temperature difference between the two sensors existed at both SAJESS locations, so we caution against the averaging of both sensors without taking these differences into account. We found similar results to Domine et al. (2021), where the RMSE between the net

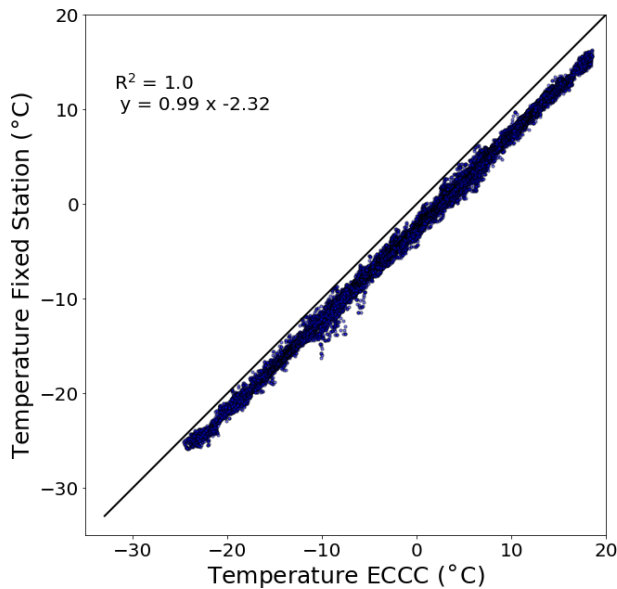


**Figure 5.** SAJESS Fixed Station and ECCC temperature data. Comparison of 1 min temperature data (63 149 recordings) from the Fixed Station temperature probe and the mean of the three ECCC temperature thermistor readings. The Fixed Station HMP155 has a  $-2.32\text{ }^{\circ}\text{C}$  bias due to the method of wiring and data recording. The solid black line represents a 1 : 1 relationship (i.e., zero bias).

radiometer (using  $\text{LW}\uparrow$ ) and the IRRs was best reduced using an unphysical emissivity ( $\varepsilon$ ) value of 1.028. This could indicate that direct comparison is difficult due to the difference in wavelength spectrum measured by the two instruments (Domine et al., 2021), yet the greater field of view of the net radiometer may also be influential. Surface temperature data have not been corrected for surface emissivity and assume  $\varepsilon = 1$  (Apogee Instruments Inc., 2022). The location of the IRRs should be installed on the unshaded south end of the cross arm in future deployment.

Snow depth measurements from the sonic ranger (SR50A) on the Fixed Station meteorological tripod were within 10 % of the values from the same type of sensor used by ECCC at the Edmundston station over the course of the 2020–2021 winter. At both SAJESS sites, the 1 min resolution caused noise in the snow depth data during periods of precipitation, which is greatly reduced using a 1 h running mean. Data from the SR50A also include a “quality number”, which is detailed in the dataset README and can be used to filter snow depth data.

The four-way net radiometers on each meteorological tripod were fitted with the heater/ventilation unit to reduce errors associated with dew/frost on the sensor window. This unit, however, does not heat the sensor window(s) sufficiently to remove snow or ice during or after precipitation, which is observed in the pyranometer data when  $\text{SW}\uparrow$  is greater than  $\text{SW}\downarrow$  and correlated with precipitation events using the disdrometer and/or snow depth data. This situation

occurred on 13 d at the Fixed Station and 5 d at the MUST Trailer. For data analysis we suggest using more advanced algorithms such as Lapo et al. (2015) to identify periods of snow accumulation, which can then be corrected with other methods available in the literature (e.g., Sicart et al., 2006; Annandale et al., 2002). Unlike Domine et al. (2021), no sustained periods of  $0.0\text{ W m}^{-2}$  are observed in the  $\text{LW}\downarrow$  data, indicating the continuous use of the ventilation unit was successful in preventing frost build-up.

#### 4.2.2 Flux tripod

Users wishing to utilize data from the flux tripod can investigate variables provided in the Flux Notes (FN), Campbell Scientific (CS), and AmeriFlux (AM) files. These include the number of  $\text{CO}_2$  and  $\text{H}_2\text{O}$  samples per averaging period and a corresponding “bad data” column. We observe that the maximum number of samples at 10 Hz for the 30 min period (18 000 in total) did not reach a total of 19.5 h during the March–April 2021 IOP. These occurrences correspond to periods of precipitation, whereby we presume the IRGASON windows were inhibited by rain/snow. On a finer scale, steady-state integral turbulence characteristic (SSITC) tests were applied to energy balance components for every 30 min period (Foken et al., 2004). These can be found in the AM files as variables named “\_SSITC\_TEST” and in the CS files as variables named “\_QC”. Users should consult Foken et al. (2004) for further information regarding these tests as further analysis is beyond the scope of the paper. Data have not been gap-filled, removed, or replaced from the dataset.

#### 4.2.3 Hotplate

Although the hotplate performed well when fully operational, a significant portion of the IOP was missed (28 March 2021 to 30 April 2021) due to faulty microprocessor settings on both hotplates (Fig. 6). These have subsequently been improved upon by the manufacturer, and further testing is underway. As described by Rasmussen et al. (2011), hotplate precipitation rate accuracy is least assured during the onset and cessation of precipitation; however, data from the hotplates include a “status” variable (no. 1, no. 2, or no. 3) that identifies these periods. A full explanation is provided with the dataset README. Precipitation data from the hotplate have not been corrected for these under- or overestimations.

Similar to Thériault et al. (2021b), we compared 30 min cumulative sums of the hotplate 1 min accumulation for December 2020–March 2021, with corrected Geonor data (using Kochendorfer et al., 2017) from the Edmundston ECCC station. These align well with the best results (reduced bias and RMSE) found for rain ( $>2\text{ }^{\circ}\text{C}$ ) and snow ( $<-2\text{ }^{\circ}\text{C}$ ). Finally, hotplate T1 (1 min average) precipitation data are more sensitive and therefore better at reproducing higher precipi-

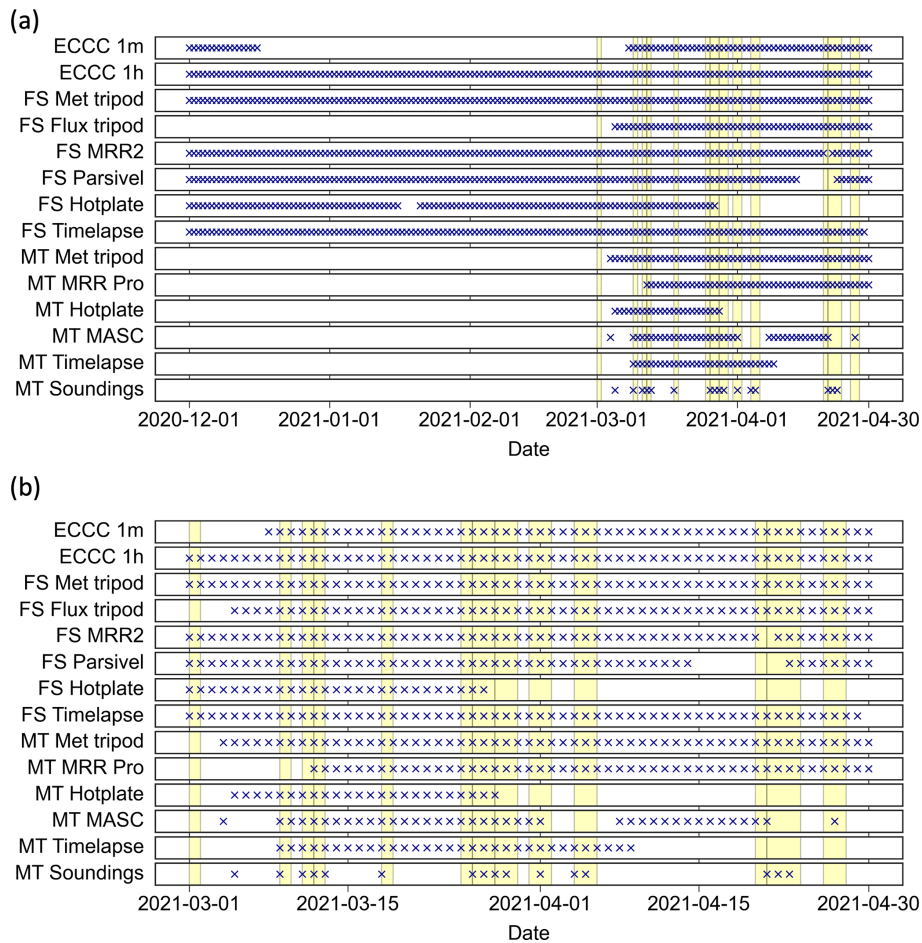


**Figure 6.** Data availability (daily resolution). Operating periods for instrumentation for (a) the entire SAJESS field campaign, 1 December 2021–30 April 2021, and (b) during the intensive observation period, 1 March 2021–30 April 2021. Data availability for the Environment and Climate Change Canada station in Edmundston is given for illustrative purposes only, as ECCC data are not included in this dataset (FS stands for Fixed Station and MT for MUST Trailer). Vertical yellow bands indicate periods of manual observations at the MUST Trailer during storm events by SAJESS volunteers and students.

tation rates than the T5 (5 min average) data, resulting in a positive bias up to  $\sim 1.5 \text{ mm h}^{-1}$  (at  $4\text{--}5 \text{ mm h}^{-1}$ ).

Due to processor issues, barometer data were not recorded by the hotplate environmental sensor at all 1 or 5 min intervals; however, valid readings do exist for each hour of the campaign. We recommend filtering barometer data from both SAJESS sites by selecting the median value during each hour to represent the hourly value. This method correlates well with ECCC station pressure reading (within 4 hPa) for the duration of the campaign. Barometer readings represent raw station pressure and are not corrected for elevation.

#### 4.2.4 Disdrometer

The disdrometer dataset contains 1039 columns, which include total particle counts for 1024 fall speed and diameter bins, and other derived variables listed in Table 4. This configuration option is provided by the OTT software as raw

data. At present we can only comment on a preliminary analysis of the OTT-derived precipitation intensity. When compared to 30 min ECCC Geonor and hotplate precipitation rates, timing and amounts from the disdrometer are generally comparable, yet we observe the Parsivel<sup>2</sup> overestimates at high precipitation rates ( $>10 \text{ mm h}^{-1}$ ), which is well documented (e.g., Angulo-Martínez et al., 2018). Users wishing to utilize the drop size and fall speed distributions, and subsequently retrieve an improved precipitation rate, can correct these data using Raupach and Berne (2015).

#### 4.2.5 Upper-air observations

Comparisons from four soundings from the MUST Trailer that aligned with either the 12:00 UTC or 00:00 UTC balloon releases from Caribou (ME) were made for data from 18, 27, and 29 March 2021, with all four sounding profiles displaying good agreement between the two sites. On some oc-

casions, surface and lower-troposphere (<700 hPa) temperatures at Edmundston were up to 5 °C lower than in Caribou, ~ 60 km to the northwest. The SAJESS sounding data also correlate well with the surface observations of precipitation type and phase. We recommend smoothing the 1 s sounding data using a low-pass filter (e.g., 10 s running mean) to remove noise in the temperature and dew point profiles.

#### 4.2.6 CoCoRaHS precipitation reports

CoCoRaHS volunteers conducted most of their observations during the IOP, due to the delays in obtaining equipment and training due to public health measures in place at the time. Despite this, 21 CoCoRaHS stations (Table 4) reported 1715 daily total precipitation (liquid-equivalent) measurements, 1729 new snow measurements, and 1123 total snow measurements (Fig. 7). A comparison of the daily precipitation and new snow amounts has not been conducted, but the total snow (i.e., snow on the ground) compares well with the Fixed Station and ECCC instruments. CoCoRaHS data are not included in the SAJESS dataset as (a) CoCoRaHS already provides long-term storage and data retrieval via its own website, and (b) the authors encourage users to explore the CoCoRaHS database for stations that may be useful for their own analysis that were not associated with SAJESS.

#### 4.2.7 MASC

The MASC captured a total of 93 343 images during March–April 2021. We present some of these images in Sect. 4.3.3, when they corroborate the particle type recorded by the manual observations. The MASC also allowed for the automated photography of particles when observers were not able to attend to manual observations or macrophotography. Users should expect, however, a large portion (perhaps 50 %) of images to not contain particles distinguishable to the naked eye. We attribute this to SAJESS representing an experimental opportunity to deploy the MASC in mixed-phase precipitation conditions. While images of liquid or freezing precipitation were usually blurred and would be considered less than ideal from an aesthetic point of view, post-processing of the images using algorithms provided in Praz et al. (2017) has resulted in particle fall speed and size distributions (similar to disdrometer results) that align well with the observed precipitation type. Analysis of the images is ongoing.

#### 4.3 Examples of data and observations

Here we provide an overview of the conditions observed during the SAJESS campaign and examples of data from each of the two SAJESS sites to illustrate possible uses. While the total SAJESS dataset is ~ 200 Gb, a ~ 1.1 Gb sample of data is available on the FRDR. This sample dataset is based on the example given here for the MUST Trailer location, where a subset of data for 18 March 2021 is dis-

played. Sample data have been made available for most instruments for the entire day (00:00–23:59 UTC) and for the MASC, macrophotography images, and the MRRs for 12:00–13:00 UTC 18 March 2023 (to reduce file size).

##### 4.3.1 Overview

Data covering 1 December 2020–30 April 2021 are provided by the instruments at the Fixed Station, which can be supplemented by the nearby ECCC station. Maximum snow depth measured at the Fixed Station was 65 cm, with snowfall amounts comparing well in timing, yet slightly less in magnitude (around 10 %), to those measured by the ECCC instruments (Fig. 7). Maximum snow depth observed at 21 surrounding CoCoRaHS stations (Table 4) ranged from 50 to 79 cm, with an average of 54 cm. During this period, the ECCC Geonor measured a total of 287 mm of (liquid-equivalent) precipitation, less than the climatological (1993–2022) mean of 364 mm.

During the IOP (8 March 2021–30 April 2021) manual observations were made during 13 storms (Fig. 6), for a total of 183 h of precipitation-type observations. Observers were present for 93 h of snow (eight storms), 63 h of rain (five storms), and 27 h of mixed precipitation (more than one phase of precipitation occurring at the same time; three storms). Two storms (12 March 2021; 4–5 April 2021) included rain–snow transitions. Observers took a total of 4483 images of precipitation particles during the IOP. Using the ECCC Geonor, observers were present for 97 mm of the 105 mm of (liquid-equivalent) precipitation that fell during the IOP period.

##### 4.3.2 Fixed Station storm measurements

Focused examples of the meteorological measurements at the Fixed Station are given in Fig. 8. This case covers the period of 25–27 December 2020 during which 22.5 h of rain on snow (14 mm) occurred from 12:30 UTC 25 December to 11:00 UTC 26 December 2020, with temperatures of 5–6 °C, reduced the Fixed Station snow depth to 0.0 m. This was followed closely by a decrease in temperature to <0 °C and ~ 4.5 h of snow (4 cm) from 16:30 to 20:50 UTC 26 December 2021, restarting the seasonal snowpack from bare conditions. Precipitation type derived from the disdrometer data correlates well with the decrease in air temperature below 0 °C. The time series of particle type can be constructed from the binned fall speed and diameter measurements and using equations in the literature such as Rasmussen et al. (1999) and Ishizaka et al. (2013) or using the precipitation-type codes produced by the instrument software (Table 2). MRR data show the reduction of melting height (determined by the sharp vertical gradient of reflectivity) from ~ 3 km a.g.l. to just over ~ 2 km a.g.l. during this same period. These insights into the evolution of the seasonal snowpack are rare as many

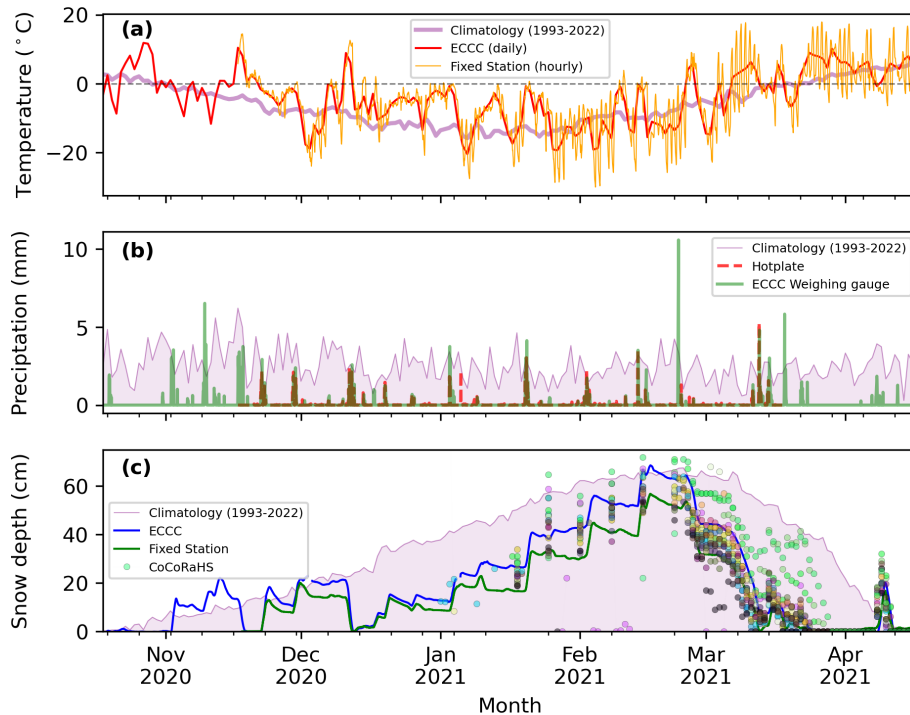


**Figure 7.** Overview of select SAJESS measurements (December 2020 to April 2021) with comparison to the Edmundston ECCC station and 1993–2022 climatology. (a) Hourly mean Fixed Station temperature (corrected, see Sect. 4.2.1), daily mean ECCC temperature, and daily mean climatology temperature. (b) Hourly accumulation from the Fixed Station hotplate precipitation gauge and ECCC weighing gauge, with daily climatology accumulation. (c) Fixed Station and ECCC snow depth measurements, 1993–2022 snow-on-the-ground climatology, and measurements from local CoCoRaHS stations listed in Table 5 (each station has a randomly assigned individual marker colour). No hotplate measurements are available, or therefore shown, for April 2021 due to an instrument fault.

standard weather or climate stations may not have the ability to explicitly identify precipitation types.

#### 4.3.3 MUST storm observations

To complement the automated measurements made at the Fixed Station, the MUST Trailer site provided observations of precipitation type, photographic imagery of particles, and upper-air soundings, in addition to the meteorological tripod and hotplate. Images and observations taken during a snow event that occurred on 18 March 2021 are shown in Figs. 9 and 10.

From 10:00 to 14:30 UTC on 18 March 2021, light, intermittent snowfall with precipitation rates between  $0.4\text{--}0.6\text{ mm h}^{-1}$  resulted in  $\sim 1.5\text{ cm}$  of snowfall at the MUST Trailer. Precipitation rates were at times so low that the hotplate did not record any precipitation, but snowfall was confirmed by the manual observations. The Fixed Station disdrometer also detected very light precipitation (maximum rate of  $0.6\text{ mm h}^{-1}$ ) with only  $0.2\text{ mm}$  total (liquid-equivalent) for the same period. The ECCC Geonor did not record any precipitation during this time. Air temperature at the MUST Trailer remained between  $-1$  and  $0^\circ\text{C}$  during most of the snowfall, with a short ( $\sim 30\text{ min}$ ) period of

snow grains being reported when temperatures increased to  $0\text{--}0.5^\circ\text{C}$ . Macrophotography images taken from the SAJESS MUST Trailer provide confirmation of hydrometeor type. From these images (Fig. 9), crystal habit, size distribution, and riming can be diagnosed, and they align with the 10 min observations that recorded overcast skies, nimbostratus clouds, and snow. Also, during this time, the MASC captured images of a variety of hydrometeors, with the clearest images being of large aggregates (Fig. 10a). At 12:00 UTC on 18 March 2021, a deep saturated layer between 900 and 700 hPa is evident on the upper-air observations from the MUST Trailer, matching the vertical profile observed in the National Weather Service (NWS) sounding from Caribou (ME) (Fig. 10b).

After a break in conditions, light precipitation made up of wet snow and rain occurred between 17:30–19:50 UTC on 18 March 2021. The mixed precipitation erased the snow collected on the snow board under the MUST Trailer SR50A. This is important as it illustrates what CoCoRaHS observers would have encountered the next morning (19 March 2021), when no observations of new snow were recorded.

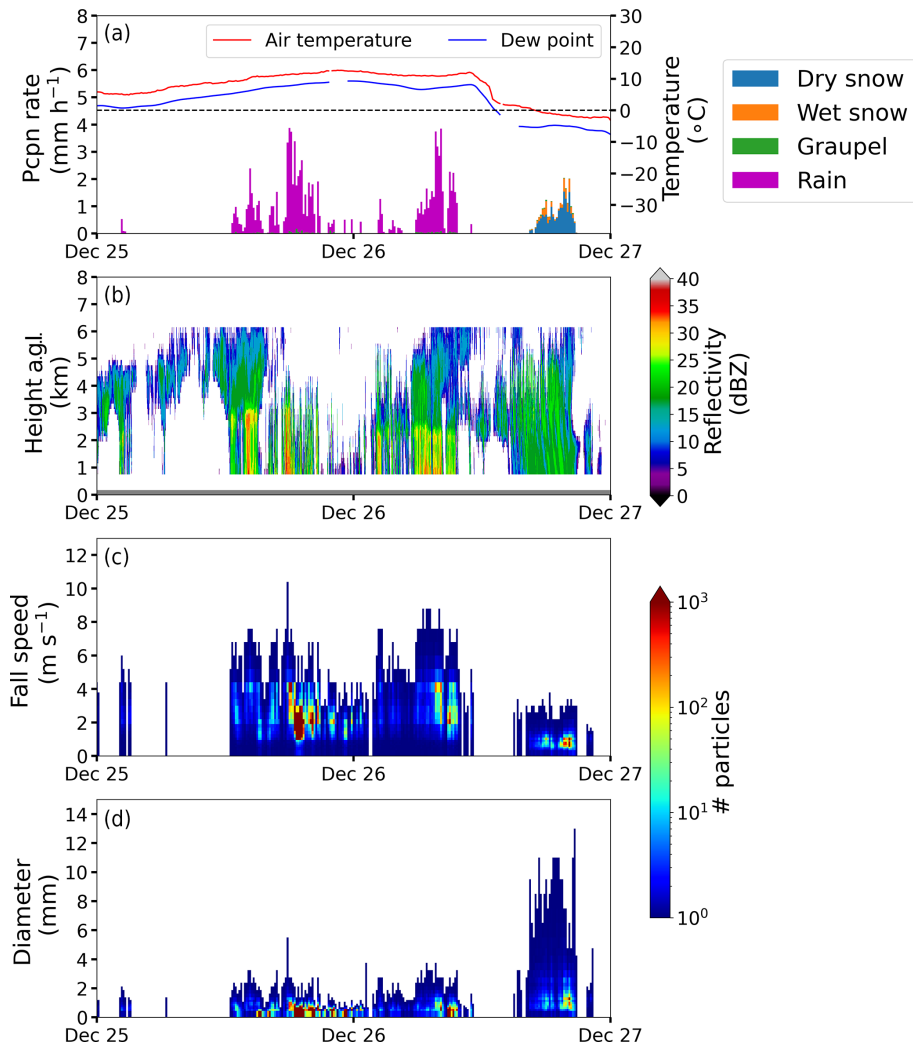


**Figure 8.** Fixed Station storm measurements. From top to bottom, (a) air temperature and precipitation. The precipitation type is derived from disdrometer data using equations in Rasmussen et al. (1999) and Ishizaka et al. (2013) and is not included in the dataset. (b) Radar reflectivity, (c) particle fall speed, and (d) diameter (both from the Parsivel disdrometer), measured at the Fixed Station from 00:00 UTC on 25 December 2020 to 23:59 UTC on 26 December 2020. Temperature, dew point, precipitation, and disdrometer data are shown as 10 min averages. Micro rain radar (MRR) data are at 10 s resolution, with a vertical resolution of 200 m.

#### 4.4 Challenges and lessons learned

Challenges during the SAJESS field campaign primarily originated from the requirement for remote computer access to monitor and troubleshoot instrument problems as they arose and intermittent interruptions to AC power, especially at the Fixed Station site.

Such issues include the requirement to restart proprietary software. For example, the disdrometer software provided by OTT requires a user to restart the program manually if the computer has suffered a power interruption or reboot. This caused some periods of missing data to be longer than necessary. For subsequent deployments, we have circumvented this issue by writing a serial-based terminal program in Python that can run on any operating system. Conversely,

software provided by METEK for the MRR will restart automatically; however, users are limited to Windows operating software.

The processor included with the MRR-Pro does allow for data collection to begin automatically, for as long as the on-board hard drive has space; however, raw data then are not retrievable as they are with the MRR2. We found this to be an adequate trade-off as the longer acquisition time per spectrum results in the MRR-Pro signal having less noise and, due to the larger number of range gates, can have a finer vertical resolution for the same maximum height as the MRR2. Our use of both versions of the METEK MRR was also due to equipment limitations within the group.

A similar restart issue arose for the hotplate, whereby a manual reset was required after the instrument's micropro-



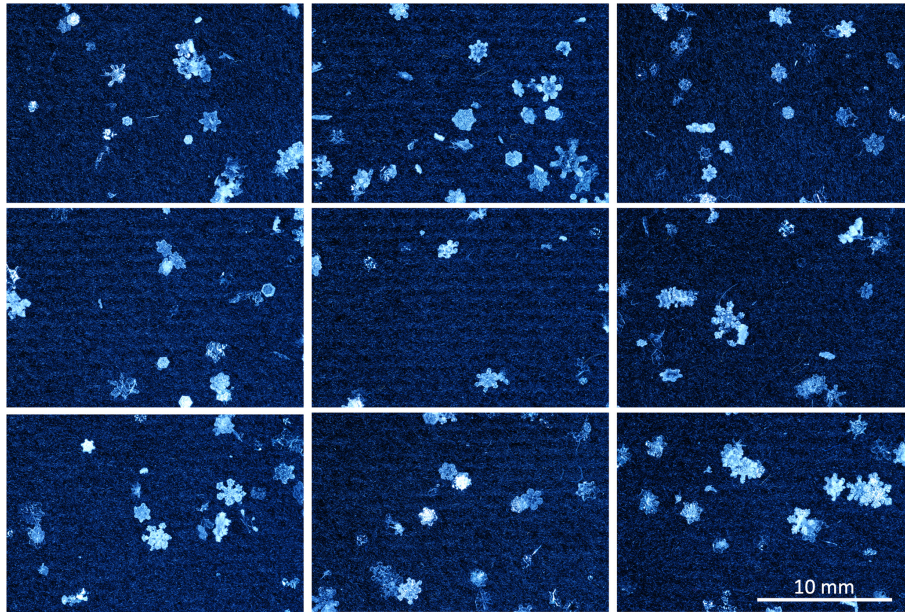


**Figure 9.** MUST Trailer macrophotography. Nine independent (i.e., no overlap) images of the felt-covered pad with solid hydrometeors collected at 12:25 UTC on 18 March 2021. Images are oriented as they were on the 13 cm  $\times$  13 cm pad.

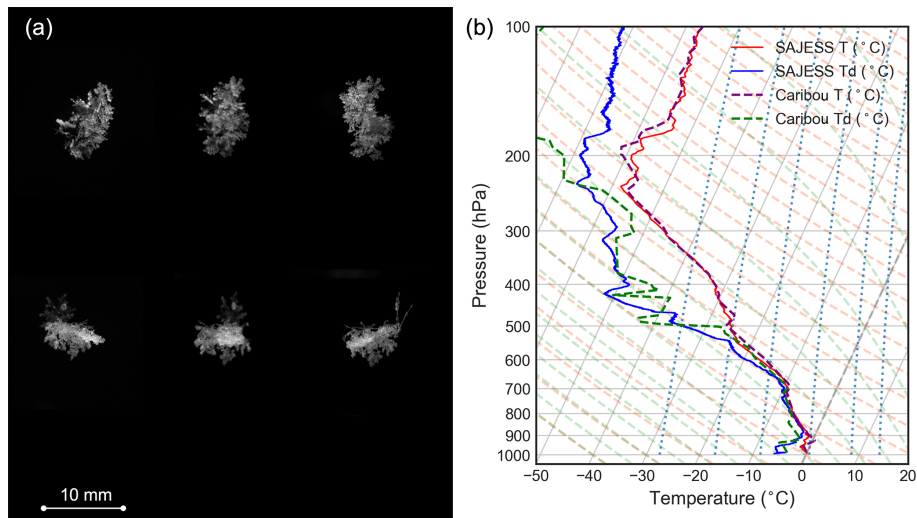


**Figure 10.** Multi-angle snowflake camera (MASC) images and upper-air observations. **(a)** Two triplet images of aggregates taken by the MASC at 12:40 UTC on 18 March 2022 and **(b)** the 12:00 UTC on 18 March 2021 soundings from the SAJESS MUST Trailer and the NWS Caribou (ME) station.

cessor cut power to the heating plates. This response has been rectified by the manufacturer; however, we have since installed a remotely controlled AC outlet to our other hot-plate stations that can be switched on/off without having to visit the site in-person.

SAJESS provided an opportunity to operate the multi-angle snowflake camera (MASC) during mixed-phased precipitation. Initial results indicate that the instrument can help diagnose mixed-phase precipitation using post-processing algorithms that determine particle fall speed and diameter to

a similar standard as the disdrometer. This leads, however, to many of the images being of blurred spherical raindrops rather than sharp pictures of ice crystal types published elsewhere. Work is ongoing to modify the post-processing software to include the categorization of raindrops, as this category is currently missing from the software.

Dishes for the SRS are required to be oriented to specific satellites (with the help of a satellite signal finder); however, it is also best if these dishes are not currently being used to receive a satellite TV signal by the household. In Edmund-

ston, we located an adequate number of unused dishes within the community; however, an SRS specific deployment may require the purchasing of new equipment solely for the purpose of the SRS. In some regions, satellite dishes may no longer be installed or maintained to a sufficient standard.

The use of community-based volunteers to assist in observations at times proved challenging, practically with respect to data quality. Our conclusion is that SAJESS could have benefited from a smaller number of high-quality measurements that could be verified, rather than a larger number of measurements that may have been prone to error. Due to public health measures in place, much of the hands-on training that was planned had to be conducted remotely, and at times restrictions limited the volunteers' access to sites and equipment. We suggest a dedicated team member to act as liaison for larger groups of volunteers. Compared to the high-temporal resolution of many of the SAJESS instruments, precipitation amounts recorded once per day may not be suitable for all analyses, as identified in Sect. 4.3.3.

Particularly difficult was the installation of the eddy-covariance flux tripod during the winter season. The burial of temperature sensors and heat flux plates was less than ideal in the frozen surface material, which also precluded a soil pit analysis and soil layer documentation. However, care was taken to ensure restoration of the soil, and turf was as complete as possible after installation. The overlying snow was also restored as homogeneously as possible to match the surrounding snowpack. Due to the lack of soil analysis, the data logger program's default bulk density value of  $1300 \text{ kg m}^{-3}$  was used. Although future deployments should not underestimate the time and energy required to install the flux instrumentation correctly, we have retained the flux data as thorough post-processing has allowed for effective analysis of the data (Leroux et al., 2023).

## 5 Data availability

The SAJESS dataset (including the sample subset of data) is available from the Federated Research Data Repository (FRDR) and can be accessed at <https://doi.org/10.20383/103.0591> (Thompson et al., 2023) and is included in the Global Water Futures FRDR collection. CoCoRaHS data are available from <https://cocorahs.org/Canada.aspx> (Colorado Climate Center, 2017). SRS data are available from the Artys' web platform (<https://www1.artys.it/>, last access: 5 December 2023) that can be accessed upon request (m.colli@artys.it). Hourly and daily data from the Edmundston ECCC station are available via the ECCC Historical data web page, with 1 min raw data from the station available from the authors upon request ([https://climate.weather.gc.ca/historical\\_data/search\\_historic\\_data\\_e.html](https://climate.weather.gc.ca/historical_data/search_historic_data_e.html), last access: 5 December 2023).

## 6 Summary

A valuable dataset was collected during the 2020–2021 Saint John River Experiment on Cold Season Storms (SAJESS) over eastern Canada. The dataset contains automatic measurements, manual observations, and photos of the meteorological conditions and precipitation at the surface, micro rain radar measurements, upper-air observations, and measurements of precipitation amounts by community volunteers.

The experiment included an intensive observation period during March–April 2021, to document conditions during the melt season with its below-average snowpack melt a month earlier than normal. The study region and downstream communities are historically prone to ice jams and flooding during late winter and early spring, which can be influenced by air temperature, rain-on-snow events, and the overall evolution of the seasonal snowpack. Despite these hazards being minimal during the campaign, the dataset will contribute to an understanding of snowpack evolution across the region by a variety of mechanisms. Firstly, the spatially distributed measurements from CoCoRaHS observers and SRS installations give a broader view of precipitation types and amounts than the typical isolated weather or climate station. The dataset contains more than 1700 measurements from these community volunteers, and the experiment doubled as a learning opportunity for the classes of school children that contributed by recording snow board and rain gauge measurements. Secondly, the identification of precipitation type at the surface, particularly when there is snow on the ground and temperatures are near  $0^\circ\text{C}$ , can be vital for forecasting the resulting snowpack and hydrological response. This was achieved during SAJESS by combining high-temporal-resolution measurements (1 min) of precipitation amount, snow depth, and disdrometer data, with manual observations and photographic imagery of hydrometeors at the surface. Verifying the precipitation type using these measurements removes the uncertainty of precipitation-type estimation that is necessary without such an array of measurements. Thirdly, observations of atmospheric conditions and precipitation aloft from the micro rain radar and upper-air soundings will advance our knowledge of pre-storm conditions and the influence of tropospheric conditions on the precipitation type observed at the surface. When these conditions result in solid precipitation at the surface, inspection of the macrophotographs and MASC images can be included to confirm particle type, size, and shape and, for snow, crystal habit and riming condition. The SAJESS dataset provides an opportunity to investigate the micro-scale influences these differing particle types and crystal habits have on snowpack evolution.

In addition, the SAJESS dataset provides the opportunity to advance forecasting and model evaluation. The breadth of instruments and human observations quantifies many parameters not archived in traditional meteorological databases. Examples of this include the non-standard timing of bal-

loon launches and spatially distributed precipitation and temperature observations, as well as energy balance and flux data. The identification of particle type obtained using non-standard observations such as the MASC provides ground truth to help further model microphysics.

Finally, the SAJESS field campaign also highlights the need to enhance measurements of precipitation and snow in the upper Saint John River basin. Near-real-time access to data during the campaign allowed for the monitoring of meteorological conditions as they occurred, which can be vital for emergency management, ice jam and flood forecasting, and river navigation. This is not usually available in areas where weather or climate stations are sparse. We envision that consideration be given to furthering the meteorological monitoring network in the upper Saint John River basin to increase the resolution and frequency of measurements and to better anticipate ice jams and major flooding events along the Saint John River.

**Author contributions.** HDT wrote the first draft of the manuscript and conducted some analyses. JMT, SJD, RES, and VV designed and led the field project. DB and LR collected manual observations during the intensive observational period. NRL contributed to the installation of the instruments and the management of the CoCoRaHS observers. MC provided the Smart Rainfall System (SRS). HDT, JMT, SJD, RES, DB, LR, NRL, MC, and VV contributed to the writing and the editing of the manuscript.

**Competing interests.** The contact author has declared that none of the authors has any competing interests.

**Disclaimer.** Publisher's note: Copernicus Publications remains neutral with regard to jurisdictional claims made in the text, published maps, institutional affiliations, or any other geographical representation in this paper. While Copernicus Publications makes every effort to include appropriate place names, the final responsibility lies with the authors.

**Acknowledgements.** Many thanks are expressed to all participants who collected measurements, provided locations for the SRS parabolic dishes, and assisted with the planning and implementation of SAJESS. We thank Jacques Doiron, Director of the Emergency Measures for the City of Edmundston, for providing the sites and facilities and coordinating the local activity with the SAJESS team, and Amanda Ronnquist for creating the SAJESS data management plan. We thank Yves-Alain Roulet (MeteoSwiss) and Alexis Berne (EPFL) for their assistance with the loan and operation of the MASC. We also thank the Digital Research Alliance of Canada and the Federated Research Data Repository for archiving the SAJESS dataset. We appreciate the detailed reviews and constructive comments provided by Siwei He, Robert Hellstrom, and two anonymous referees and the assistance of the editor, David Carlson.

**Financial support.** Funding was provided by the Global Water Futures programme, which is project 418474-1234 funded by the Canada First Research Excellence Fund, Natural Sciences and Engineering Research Council of Canada Discovery Grants (Julie M. Thériault, Stephen J. Déry, and Ronald E. Stewart), the Canada Research Chairs Program (Julie M. Thériault), and University of Northern British Columbia (Lisa Rickard), to conduct scientific analysis. The MUST Trailer was developed with funding from the Canada Foundation for Innovation.

**Review statement.** This paper was edited by David Carlson and reviewed by Robert Hellstrom and two anonymous referees.

## References

- Angulo-Martínez, M., Beguería, S., Latorre, B., and Fernández-Raga, M.: Comparison of precipitation measurements by OTT Parsivel<sup>2</sup> and Thies LPM optical disdrometers, *Hydrol. Earth Syst. Sci.*, 22, 2811–2837, <https://doi.org/10.5194/hess-22-2811-2018>, 2018.
- Annandale, J., Jovanovic, N., Benadé, and N., Allen, R.: Software for missing data error analysis of Penman-Monteith reference evapotranspiration, *Irrigation Sci.*, 21, 57–67, <https://doi.org/10.1007/s002710100047>, 2002.
- Apogee Instruments Inc.: Infrared radiometers owner's manual, <https://www.apogeeinstruments.com/content/SI-400-manual.pdf> (last access: 9 March 2023), 2022.
- Beltaos, S., Ismail, S., and Burrell, B.: Midwinter breakup and jamming on the upper Saint John River: A case study, *Can. J. Civil Eng.*, 30, 77–88, <https://doi.org/10.1139/102-062>, 2003.
- Budhathoki, S., Rokaya, P., and Lindenschmidt, K. E.: Impacts of future climate on the hydrology of a transboundary river basin in northeastern North America, *J. Hydrol.*, 605, 127317, <https://doi.org/10.1016/j.jhydrol.2021.127317>, 2022.
- Buttle, J. M., Allen, D. M., Caissie, D., Davison, B., Hayashi, M., Peters, D. L., Pomeroy, J. W., Simonovic, S., St-Hilaire, A., and Whitfield, P. H.: Flood processes in Canada: Regional and special aspects, *Can. Water Resour. J.*, 41, 7–30, <https://doi.org/10.1080/07011784.2015.1131629>, 2016.
- Campbell Scientific: IRGASON: Integrated CO<sub>2</sub>/H<sub>2</sub>O Open Path Gas Analyzer and 3-D Sonic Anemometer, <https://s.campbellsci.com/documents/us/manuals/irgason.pdf> (last access: 5 December 2023), 2022a.
- Campbell Scientific: EASYFLUX DL: EASYFLUX DL CR6OP or CR1KXOP For CR6 or CR1000X and Open-Path Eddy-Covariance Systems. Retrieved August 31, 2022, <https://s.campbellsci.com/documents/us/manuals/easyflux-dl-cr6op.pdf> (last access: 6 September 2023), 2022b.
- Cauteruccio, A., Chinchella, E., Stagnaro, M., and Lanza, L. G.: Snow particle collection efficiency and adjustment curves for the hotplate precipitation gauge, *J. Hydrometeorol.*, 22, 941–954, <https://doi.org/10.1175/JHM-D-20-0149.1>, 2021.
- Cifelli, R., Doesken, N., Kennedy, P., Carey, L. D., Rutledge, S. A., Gimmestad, C., and Depue, T.: The Community Collaborative Rain, Hail, and Snow Network: Informal education for scientists and citizens, *B. Am. Meteorol. Soc.*, 86, 1069–1077, <http://www.jstor.org/stable/26221344> (last access: 5 December 2023), 2005.

- Colli, M., Stagnaro, M., Caridi, A., Lanza, L.G., Randazzo, A., Pastorino, M., Caviglia, D.D., and Delucchi, A.: A Field Assessment of a rain estimation system based on satellite-to-earth microwave links, *IEEE T. Geosci. Remote*, 57, 2864–2875, <https://doi.org/10.1109/TGRS.2018.2878338>, 2019.
- Colli, M., Cassola, F., Martina, F., Trovatore, E., Delucchi, A., Maggiolo, S., and Caviglia, D.D.: Rainfall fields monitoring based on satellite microwave down-links and traditional techniques in the city of Genoa, *IEEE T. Geosci. Remote*, 58, 6266–6280, <https://doi.org/10.1109/TGRS.2020.2976137>, 2020.
- Colorado Climate Center: Community collaborative rain, hail & snow network, CoCoRaHS Canada [data set], <https://cocorahs.org/Canada.aspx> (last access: 15 March 2022), 2017.
- Domine, F., Lackner, G., Sarrazin, D., Poirier, M., and Belke-Brea, M.: Meteorological, snow and soil data (2013–2019) from a herb tundra permafrost site at Bylot Island, Canadian high Arctic, for driving and testing snow and land surface models, *Earth Syst. Sci. Data*, 13, 4331–4348, <https://doi.org/10.5194/essd-13-4331-2021>, 2021.
- Environment and Climate Change Canada (ECCC): Top ten weather stories for 2008: story four: Saint John River floods from top to bottom, <https://www.ec.gc.ca/meteo-weather/default.asp?lang=En&n=7D6FDB7C-1> (last access: 25 March 2023), 2017.
- Environment and Climate Change Canada (ECCC): Canada's top 10 weather stories of 2018: 7. Flash flooding of the Saint John River, <https://www.canada.ca/en/environment-climate-change/services/top-ten-weather-stories/2018.html#toc6> (last access: 25 March 2023), 2019.
- Environment and Climate Change Canada (ECCC): Canada's top 10 weather stories of 2019: 9. Saint John River floods again, <https://www.canada.ca/en/environment-climate-change/services/top-ten-weather-stories/2019.html#toc10> (last access: 25 March 2023), 2020.
- Falconi, M. T., von Lerber, A., Ori, D., Marzano, F. S., and Moisseev, D.: Snowfall retrieval at X, Ka and W bands: consistency of backscattering and microphysical properties using BAecc ground-based measurements, *Atmos. Meas. Tech.*, 11, 3059–3079, <https://doi.org/10.5194/amt-11-3059-2018>, 2018.
- Fitch, K. E., Hang, C., Talaei, A., and Garrett, T. J.: Arctic observations and numerical simulations of surface wind effects on Multi-Angle Snowflake Camera measurements, *Atmos. Meas. Tech.*, 14, 1127–1142, <https://doi.org/10.5194/amt-14-1127-2021>, 2021.
- Foken, T., Göockede, M., Mauder, M., Mahrt, L., Amiro, B., and Munger, W.: Post-Field Data Quality Control, in: *Handbook of Micrometeorology, Atmospheric and Oceanographic Sciences Library*, edited by: Lee, X., Massman, W., and Law, B., vol. 29, Springer, Dordrecht, [https://doi.org/10.1007/1-4020-2265-4\\_9](https://doi.org/10.1007/1-4020-2265-4_9), 2004.
- Fortin, G., and Dubreuil, V.: A geostatistical approach to create a new climate types map at regional scale: case study of New Brunswick, Canada, *Theor. Appl. Climatol.*, 139, 323–334, <https://doi.org/10.1007/s00704-019-02961-2>, 2020.
- Garrett, T. J., Fallgatter, C., Shkurko, K., and Howlett, D.: Fall speed measurement and high-resolution multi-angle photography of hydrometeors in free fall, *Atmos. Meas. Tech.*, 5, 2625–2633, <https://doi.org/10.5194/amt-5-2625-2012>, 2012.
- Giannetti, F. and Reggiannini, R.: Opportunistic rain rate estimation from measurements of satellite downlink attenuation: A survey, *Sensors*, 21, 5872, <https://doi.org/10.3390/s21175872>, 2021.
- Gibson, S. R. and Stewart, R. E.: Observations of ice pellets during a winter storm, *Atmos. Res.*, 85, 64–76, <https://doi.org/10.1016/j.atmosres.2006.11.004>, 2007.
- Hauser, D., Amayenc, P., Nutten, B., and Waldteufel, P.: A New Optical Instrument for Simultaneous Measurement of Raindrop Diameter and Fall Speed Distributions, *J. Atmos. Ocean. Tech.*, 1, 256–269, [https://doi.org/10.1175/1520-0426\(1984\)001<0256:ANOIFS>2.0.CO;2](https://doi.org/10.1175/1520-0426(1984)001<0256:ANOIFS>2.0.CO;2), 1984.
- Hicks, A. and Notaroš, B. M.: Method for classification of snowflakes based on images by a multi-angle snowflake camera using convolutional neural networks, *J. Atmos. Ocean. Tech.*, 36, 2267–2282, <https://doi.org/10.1175/JTECH-D-19-0055.1>, 2019.
- Houze, R. A., McMurdie, L. A., Petersen, W. A., Schwall Er, M. R., Baccus, W., Lundquist, J. D., Mass, C. F., Nijssen, B., Rutledge, S. A., Hudak, D. R., Tanelli, S., Mace, G. G., Poellot, M. R., Lettenmaier, D. P., Zagrodnik, J. P., Rowe, A. K., DeHart, J. C., Madaus, L. E., and Barnes, H. C.: The olympic mountains experiment (Olympex), *B. Am. Meteorol. Soc.*, 98, 2167–2188, <https://doi.org/10.1175/BAMS-D-16-0182.1>, 2017.
- Ishizaka, M., Motoyoshi, H., Nakai, S., Shiina, T., Kumakura, T., and Muramoto, K. I.: A new method for identifying the main type of solid hydrometeors contributing to snowfall from measured size-fall speed relationship, *J. Meteorol. Soc. Jpn.*, 91, 747–762, <https://doi.org/10.2151/jmsj.2013-602>, 2013.
- Joe, P., Scott, B., Doyle, C., Isaac, G., Gultepe, I., Forsyth, D., Cober, S., Campos, E., Heckman, I., Donaldson, N., Hudak, D., Rasmussen, R., Kucera, P., Stewart, R., Thériault, J. M., Fisco, T., Rasmussen, K. L., Carmichael, H., Laplante, A., Bailey, M., and Boudala, F.: The Monitoring Network of the Vancouver 2010 Olympics, *Pure Appl. Geophys.*, 171, 25–58, <https://doi.org/10.1007/s00024-012-0588-z>, 2014.
- Kenny, J. L. and Secord, A. G.: Engineering modernity: Hydroelectric development in New Brunswick, 1945–1970, *Acadiensis*, 39, 3–26, 2010.
- Kochendorfer, J., Rasmussen, R., Wolff, M., Baker, B., Hall, M. E., Meyers, T., Landolt, S., Jachcik, A., Isaksen, K., Brækkan, R., and Leeper, R.: The quantification and correction of wind-induced precipitation measurement errors, *Hydrol. Earth Syst. Sci.*, 21, 1973–1989, <https://doi.org/10.5194/hess-21-1973-2017>, 2017.
- Liao, L., Meneghini, R., Tokay, A., and Bliven, L. F.: Retrieval of snow properties for Ku- and Ka-band dual-frequency radar, *J. Appl. Meteorol. Clim.*, 55, 1845–1858, <https://doi.org/10.1175/JAMC-D-15-0355.1>, 2016.
- Lapo, K. E., Hinkelman, L. M., Landry, C. C., Massmann, A. K., and Lundquist, J. D.: A simple algorithm for identifying periods of snow accumulation on a radiometer, *Water Resour. Res.*, 51, 7820–7828, <https://doi.org/10.1002/2015WR017590>, 2015.
- Leroux, N. R., Vionnet, V., and Thériault, J. M.: Performance of precipitation phase partitioning methods and their impact on snow-pack evolution in a humid continental climate, *Hydrol. Process.*, 37, 1–18, <https://doi.org/10.1002/hyp.15028>, 2023.
- Löffler-Mang, M. and Joss, J.: An optical disdrometer for measuring size and velocity of hydrometeors, *J. Atmos. Ocean. Tech.*, 17, 130–139, [https://doi.org/10.1175/1520-0426\(2000\)017<0130:AODFMS>2.0.CO;2](https://doi.org/10.1175/1520-0426(2000)017<0130:AODFMS>2.0.CO;2), 2000.

- Maahn, M. and Kollias, P.: Improved Micro Rain Radar snow measurements using Doppler spectra post-processing, *Atmos. Meas. Tech.*, 5, 2661–2673, <https://doi.org/10.5194/amt-5-2661-2012>, 2012.
- Marwitz, J.: A comparison of winter orographic storms over the San Juan Mountains and the Sierra Nevada, *Meteor. Mon.*, 43, 109–114, <https://doi.org/10.1175/0065-9401-21.43.109>, 1986.
- McMurdie, L. A., Heymsfield, G. M., Yorks, J. E., Braun, S. A., Skofronick-Jackson, G., Rauber, R. M., Yuter, S., Colle, B., McFarquhar, G. M., Poellot, M., Novak, D. R., Lang, T. J., Kroodsma, R., McLinden, M., Oue, M., Kollias, P., Kumjian, M. R., Greybush, S. J., Heymsfield, A. J., Finlon, J. A., McDonald, V. L., and Nicholls, S.: Chasing Snowstorms: The Investigation of Microphysics and Precipitation for Atlantic Coast-Threatening Snowstorms (IMPACTS) Campaign, *B. Am. Meteorol. Soc.*, 103, E1243–E1269, <https://doi.org/10.1175/BAMS-D-20-0246.1>, 2022.
- METEK: Micro Rain Radar MRR-PRO, [https://metek.de/wp-content/uploads/2016/12/20180206\\_Datenblatt\\_MRR-PRO.pdf](https://metek.de/wp-content/uploads/2016/12/20180206_Datenblatt_MRR-PRO.pdf) (last access: 22 June 2022), 2017.
- Newton, B. and Burrell, B. C.: The April–May 2008 flood event in the Saint John River Basin: Causes, assessment, and damages, *Can. Water Resour. J.*, 41, 118–128, <https://doi.org/10.1080/07011784.2015.1009950>, 2016.
- Nitu, R., Roulet, Y.-A., Wolff, M., Earle, M., Reverdin, A., Smith, C., Kochendorfer, J., Morin, S., Rasmussen, R., Wong, K., Alastrué, J., Arnold, L., Baker, B., Buisan, S., Collado, J. L., Colli, M., Collins, B., Gaydos, A., Hannula, H.-R., J. Hoover, Joe, P., Kontu, A., Laine, T., Lanza, L., Lanzinger, E., Lee, G. W., Lejeune, Y., Leppänen, L., Mekis, E., Panel, J.-M., Poikonen, A., Ryu, S., Sabatini, F., Theriault, J., Yang, D., Genthon, C., van den Heuvel, F., Hirasawa, N., Konishi, H., Motoyoshi, H., Nakai, S., Nishimura, K., Senese, A., and Yamashita, K.: WMO Solid Precipitation Intercomparison Experiment (SPICE) (2012–2015), Report 131, World Meteorological Organization, 1429 pp., [https://library.wmo.int/doc\\_num.php?explnum\\_id=5686](https://library.wmo.int/doc_num.php?explnum_id=5686) (last access: 5 December 2023), 2018.
- Onset Computer Corporation: Hobo temperature/RH data logger, HOBO Temperature/RH Data Logger MX2301A | Onset Data Loggers, <https://www.onsetcomp.com/products/data-loggers/mx2301a/>, last access: 15 March 2022.
- OTT: Operating instructions Present Weather Sensor OTT Parsivel<sup>2</sup>, <https://www.ott.com/download/operating-instructions-present-weather-sensor-ott-parsivel2-with-screen-heating-2/> (last access: 5 September 2023), 2019.
- Pond Engineering: K63 Hotplate total precipitation gauge, <http://www.pondengineering.com/k63> (last access: 25 March 2023), 2021.
- Praz, C., Roulet, Y.-A., and Berne, A.: Solid hydrometeor classification and riming degree estimation from pictures collected with a Multi-Angle Snowflake Camera, *Atmos. Meas. Tech.*, 10, 1335–1357, <https://doi.org/10.5194/amt-10-1335-2017>, 2017.
- Rasmussen, R. M., Vivekanandan, J., Cole, J., Myers, B., and Masters, C.: The estimation of snowfall rate using visibility, *J. Appl. Meteorol.*, 38, 1542–1563, [https://doi.org/10.1175/1520-0450\(1999\)038<1542:TEOSRU>2.0.CO;2](https://doi.org/10.1175/1520-0450(1999)038<1542:TEOSRU>2.0.CO;2), 1999.
- Rasmussen, R. M., Hallett, J., Purcell, R., Landolt, S. D., and Cole, J.: The hotplate precipitation gauge, *J. Atmos. Ocean. Tech.*, 28, 148–164, <https://doi.org/10.1175/2010JTECHA1375.1>, 2011.
- Raupach, T. H. and Berne, A.: Correction of raindrop size distributions measured by Parsivel disdrometers, using a two-dimensional video disdrometer as a reference, *Atmos. Meas. Tech.*, 8, 343–365, <https://doi.org/10.5194/amt-8-343-2015>, 2015.
- Reges, H. W., Doesken, N., Turner, J., Newman, N., Bergantino, A., and Schwalbe, Z.: CoCoRaHS: The evolution and accomplishments of a volunteer rain gauge network, *B. Am. Meteorol. Soc.*, 97, 1831–1846, <https://doi.org/10.1175/BAMS-D-14-00213.1>, 2016.
- Schaer, M., Praz, C., and Berne, A.: Identification of blowing snow particles in images from a Multi-Angle Snowflake Camera, *The Cryosphere*, 14, 367–384, <https://doi.org/10.5194/tc-14-367-2020>, 2020.
- Sicart, J. E., Pomeroy, J. W., Essery, R. L. H., and Bewley, D.: Incoming longwave radiation to melting snow: observations, sensitivity and estimation in Northern environments, *Hydrol. Process.*, 20, 3697–3708, <https://doi.org/10.1002/hyp.6383>, 2006.
- Skofronick-Jackson, G., Hudak, D., Petersen, W., Nesbitt, S. W., Chandrasekar, V., Durden, S., Gleicher, K. J., Huang, G. J., Joe, P., Kollias, P., Reed, K. A., Schwaller, M. R., Stewart, R., Tanelli, S., Tokay, A., Wang, J. R., and Wolde, M.: Global precipitation measurement cold season precipitation experiment (GCPEX): For measurement’s sake, let it snow, *B. Am. Meteorol. Soc.*, 96, 1719–1741, <https://doi.org/10.1175/BAMS-D-13-00262.1>, 2015.
- Souvereinjs, N., Gossart, A., Lhermitte, S., Gorodetskaya, I. V., Kneifel, S., Maahn, M., Bliven, F. L., and van Lipzig, N. P. M.: Estimating radar reflectivity – Snowfall rate relationships and their uncertainties over Antarctica by combining disdrometer and radar observations, *Atmos. Res.*, 196, 211–223, <https://doi.org/10.1016/j.atmosres.2017.06.001>, 2017.
- Stewart, R. E.: Canadian Atlantic Storms Program: Progress and plans of the meteorological component, *B. Am. Meteorol. Soc.*, 72, 364–371, [https://doi.org/10.1175/1520-0477\(1991\)072<0364:CASPPA>2.0.CO;2](https://doi.org/10.1175/1520-0477(1991)072<0364:CASPPA>2.0.CO;2), 1991.
- Stewart, R. E., Shaw, R. W., and Isaac, G. A.: Canadian Atlantic Storms Program: The meteorological field project, *B. Am. Meteorol. Soc.*, 68, 338–345, <http://www.jstor.org/stable/26225054> (last access: 5 December 2023), 1987.
- Theriault, J. M., Hung, I., Vaquer, P., Stewart, R. E., and Pomeroy, J. W.: Precipitation characteristics and associated weather conditions on the eastern slopes of the Canadian Rockies during March–April 2015, *Hydrol. Earth Syst. Sci.*, 22, 4491–4512, <https://doi.org/10.5194/hess-22-4491-2018>, 2018.
- Theriault, J. M., Déry, S. J., Pomeroy, J. W., Smith, H. M., Almonte, J., Bertoncini, A., Crawford, R. W., Desroches-Lapointe, A., Lachapelle, M., Mariani, Z., Mitchell, S., Morris, J. E., Hébert-Pinard, C., Rodriguez, P., and Thompson, H. D.: Meteorological observations collected during the Storms and Precipitation Across the continental Divide Experiment (SPADE), April–June 2019, *Earth Syst. Sci. Data*, 13, 1233–1249, <https://doi.org/10.5194/essd-13-1233-2021>, 2021a.
- Theriault, J. M., Leroux, N. R., and Rasmussen, R. M.: Improvement of solid precipitation measurements using a hotplate precipitation gauge, *J. Hydrometeorol.*, 22, 877–885, <https://doi.org/10.1175/JHM-D-20-0168.1>, 2021b.
- Theriault, J. M., Leroux, N. R., Stewart, R. E., Bertoncini, A., Déry, S. J., Pomeroy, J. W., Thompson, H. D., Smith, H., Mari-

- ani, Z., Desroches-Lapointe, A., Mitchell, S., and Almonte, J.: Storms and Precipitation across the continental Divide Experiment (SPADE), *B. Am. Meteorol. Soc.*, 103, E2628–E2649, <https://doi.org/10.1175/BAMS-D-21-0146.1>, 2022.
- Thompson, H. D., Thériault, J. M., Déry, S. J., Stewart, R. E., Boisvert, D., Rickard, L., Leroux, N. R., Colli, M., and Vincent Vionnet, V.: Atmospheric and surface observation data collected during the Saint John River Experiment on Cold Season Storms, Federated Research Data Repository [data set], <https://doi.org/10.20383/103.0591>, 2023.
- Tokay, A., Hartmann, P., Battaglia, A., Gage, K. S., Clark, W. L., and Williams, C. R.: A field study of reflectivity and Z-R relations using vertically pointing radars and disdrometers, *J. Atmos. Ocean. Technol.*, 26, 1120–1134, <https://doi.org/10.1175/2008JTECHA1163.1>, 2009.
- US Department of Energy: FLUXNET: The Data Portal Serving the FLUXNET Community, <https://fluxnet.org/2017/10/10/toolbox-a-rolling-list-of-softwarepackages-for-flux-related-data-processing/> (last access: 31 August 2022), 2021.